Divergent receptor proteins confer responses to different karrikins in two ephemeral weeds

Yueming Kelly Sun[1,2], Adrian Scaffidi[1], Jiaren Yao[1], Kim Melville[1], Steven M Smith[3,4], Gavin R Flematti[1] and Mark T Waters[1,2,5]

1. School of Molecular Sciences, The University of Western Australia, 35 Stirling Hwy, Perth, WA 6009, Australia
2. Australian Research Council Centre of Excellence in Plant Energy Biology, The University of Western Australia, 35 Stirling Hwy, Perth, WA 6009, Australia
3. School of Natural Sciences, The University of Tasmania, Hobart, TAS 7000, Australia
4. Institute of Genetics and Developmental Biology, Chinese Academy of Sciences, 1 West Beichen Road, Beijing 100101, PR China.
5. Author for correspondence: mark.waters@uwa.edu.au

Word count (Abstract, main text and methods): 5143 words

ABSTRACT

Wildfires can encourage the establishment of invasive plants by releasing potent germination stimulants, such as karrikins. Seed germination of *Brassica tournefortii*, a noxious weed of Mediterranean climates, is strongly stimulated by KAR_1, which is the most abundant karrikin produced from burning vegetation. In contrast, the closely-related yet non-fire-associated ephemeral *Arabidopsis thaliana* responds preferentially to the less abundant KAR_2. The α/β-hydrolase KARRIKIN INSENSITIVE2 (KAI2) is the putative karrikin receptor identified in *Arabidopsis*. Here we show that *B. tournefortii* differentially expresses three *KAI2* homologues, and the most highly-expressed homologue is sufficient to confer enhanced responses to KAR_1 relative to KAR_2 when expressed in *Arabidopsis*. We further identify two variant amino acid residues near the KAI2 active site that explain the ligand selectivity. Our results suggest that duplication and diversification of KAI2 proteins could confer upon weedy ephemerals differential responses to chemical cues produced by environmental disturbance, including fire. (146 words)

INTRODUCTION

Environmental disturbance promotes the establishment of invasive species, posing a potent threat to global biodiversity. Changing wildfire regimes, such as increasing frequency of fires, is one of the most relevant disturbance factors contributing to elevated invasion threat[1]. Wildfires create germination opportunities in part by releasing seed germination stimulants, such as karrikins, from burning vegetation[2, 3]. Karrikins comprise a family of butenolides with six known members. In samples of smoke water generated by burning grass straw, KAR_1 is the most abundant karrikin, while KAR_2 is six times less abundant[4]. These two analogues differ only by the presence of a methyl group on the butenolide ring in KAR_1, which is absent in KAR_2 (Supplementary Fig. 1a). Invasive plant species that are responsive to karrikins could utilise natural and human-induced fires to facilitate their establishment[5, 6].

Brassica tournefortii (Brassicaceae; Sahara mustard) is native to northern Africa and the Middle East, but is an invasive weed that blights many ecosystems with a Mediterranean climate and chaparral-type vegetation that are prone to wildfires in North America, Australia and South Africa. *B. tournefortii* seed can persist in the soil for many seasons, undergoing wet-dry cycling that can influence dormancy and contribute to boom-bust cycles that outcompete native

46 species[7, 8]. *B. tournefortii* plants may radically alter fire frequency and intensity by influencing
47 fuel profiles[9, 10], further exacerbating the impact of fire on susceptible native ecosystems. In
48 addition, seed of *B. tournefortii* is particularly responsive to smoke-derived karrikins, and
49 shows a positive germination response to KAR_1 in the nanomolar range[11]. Accordingly, *B.*
50 *tournefortii* is particularly well positioned to invade areas disturbed by fire events[12, 13].

51 The putative karrikin receptor KARRIKIN INSENSITIVE 2 (KAI2) was identified in *Arabidopsis*
52 *thaliana*, a weedy ephemeral that originated in Eurasia but is now widely distributed
53 throughout the northern hemisphere[14, 15, 16]. Arabidopsis is not known to colonise fire-prone
54 habitats, but nevertheless seeds germinate in response to karrikins in the micromolar range[17].
55 Unlike most smoke-responsive species that respond more readily to KAR_1[18, 19], Arabidopsis
56 responds preferentially to the less abundant analogue KAR_2[17]. KAI2 is an evolutionarily ancient
57 α/β-hydrolase and a paralogue of DWARF14 (D14), the receptor for strigolactones[20, 21].
58 Karrikins and strigolactones are chemically similar by virtue of a butenolide moiety that is
59 necessary for bioactivity[22, 23]. KAI2 and D14 have dual functions as both enzyme and receptor,
60 but the functional significance of the enzymatic activity remains contested[24, 25, 26, 27, 28].
61 Furthermore, the basis for ligand specificity by these two highly congruent proteins remains
62 essentially unknown.

63 Orthologues of *KAI2* are ubiquitous in land plants, and are normally present as a single gene
64 copy within an ancient and highly conserved "eu-KAI2" clade[29]. There is growing evidence that,
65 beyond its ability to mediate karrikin responses, KAI2 has a core ancestral role in perceiving an
66 endogenous karrikin-like ligand ("KL") that regulates seed germination, seedling development,
67 leaf shape and cuticle development[30, 31, 32]. Since its divergence from the Arabidopsis lineage,
68 the tribe Brassiceae, which includes the genus *Brassica*, underwent a whole genome triplication
69 event 24–29 million years ago[33, 34, 35]. This process might have allowed additional KAI2 copies
70 to gain altered ligand specificity, potentially enhancing perception of environmental signals
71 such as karrikins from smoke. Here, we report that two KAI2 homologues expressed in *B.*
72 *tournefortii* show distinct preferences for different karrikins. We take advantage of the
73 relatively recent genome triplication event in the Brassiceae to identify two amino acids that
74 are sufficient to explain these karrikin preferences and confirm this by mutagenesis. Beyond
75 demonstrating the potential ecological significance of diversity among KAI2 homologues, our
76 findings also reveal active site regions critical for ligand selectivity in the broader family of
77 KAI2–D14 receptor-enzymes.

RESULTS

B. tournefortii is most sensitive to KAR_1

To characterise the karrikin response of *B. tournefortii*, we performed multiple physiological and molecular assays comparing KAR_1 activity with that of KAR_2. First, germination of *B. tournefortii* seeds was consistently more responsive to KAR_1 than KAR_2 at 10 nM, 100 nM and 1 µM (Fig. 1a and Supplementary Fig. 1b-d). Second, homologues of two karrikin-responsive transcripts, *D14-LIKE2* (*BtDLK2*) and *SALT TOLERANCE HOMOLOG7* (*BtSTH7*), required ten-fold higher concentrations of KAR_2 (1 µM) compared with KAR_1 (100 nM) to reach equivalent levels (Fig. 1b). These observed differences in seed response are not due to differential karrikin uptake, since both KAR_1 and KAR_2 were taken up from solution at similar rates by *B. tournefortii* seeds during imbibition, as was also true for Arabidopsis seeds (Supplementary Fig. 1e-f). Besides promoting germination of primary dormant seeds, karrikins also inhibited hypocotyl elongation in *B. tournefortii* seedlings, as is the case in Arabidopsis; again, KAR_1 showed a stronger effect than KAR_2 (Fig. 1c-d). Expression of *BtDLK2* transcripts in seedlings was also more responsive to KAR_1 than KAR_2 at a given concentration (Fig. 1e). Therefore, we conclude that *B. tournefortii* is more sensitive to KAR_1 than to KAR_2, a ligand preference that is a feature of many karrikin-responsive species from ecosystems prone to fires[18, 19].

Two *B. tournefortii* KAI2 homologues are functional in Arabidopsis

To establish whether there are multiple *KAI2* homologues present in *B. tournefortii*, we examined transcriptomes from seeds and seedlings. Three putative *KAI2* homologues were identified (*BtKAI2a*, *BtKAI2b*, and *BtKAI2c*; Fig. 2a; Supplementary Fig. 2 and 3). *BtKAI2a* grouped with *AtKAI2* and those of other Brassicaceae within a single clade, whereas *BtKAI2b* and *BtKAI2c* grouped within a clade unique to *Brassica*. This phylogenetic pattern implies that *BtKAI2a* is the ancestral copy of *KAI2*, whereas *BtKAI2b* and *BtKAI2c* presumably arose more recently via genome triplication during the evolution of *Brassica*. All three *BtKAI2* transcripts were expressed in *B. tournefortii* seeds, but only *BtKAI2a* and *BtKAI2b* could be detected in seedlings (Fig. 2b). Across seed and seedlings, *BtKAI2b* transcripts were the most abundant of the three, but there were no consistent effects on any of the transcripts by treatment with 1 µM KAR_1. We also identified two *BtD14* homologues, at least one of which is functionally orthologous to *AtD14* (Supplementary Figs. 2 and 4).

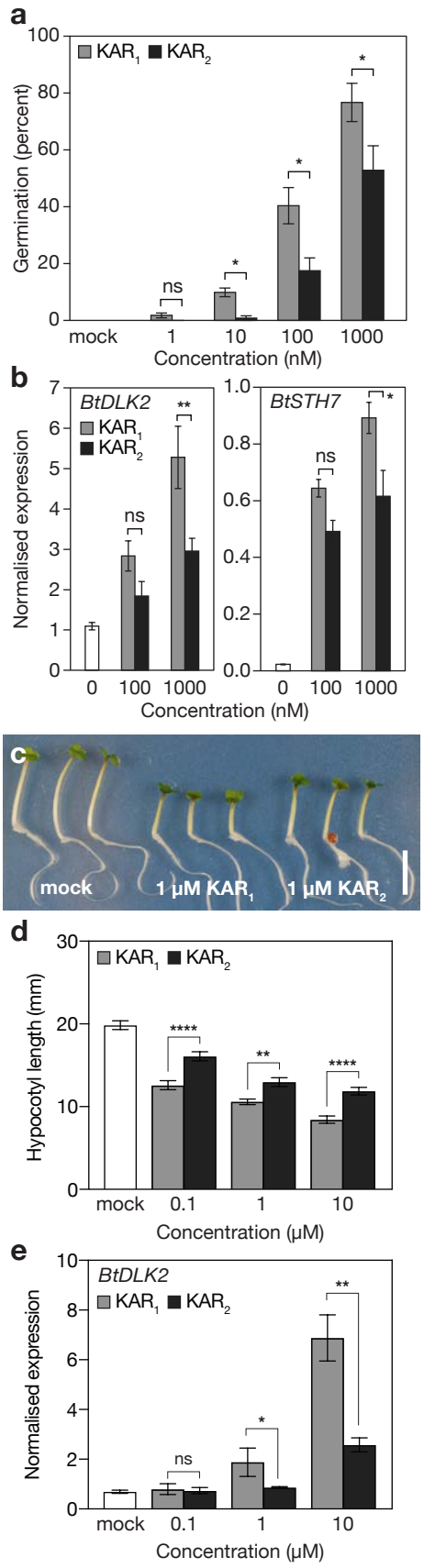

Figure 1. *Brassica tournefortii* is most sensitive to KAR_1, the major karrikin analogue isolated from plant-derived smoke

a, Germination responses of *B. tournefortii* seed to KAR_1 and KAR_2. Data are cumulative germination after 11 days (means ± SE; *n* = 3 biological replicates per treatment, ≥35 seeds per replicate). **b**, Levels of karrikin-responsive transcripts *BtDLK2* and *BtSTH7* in *B. tournefortii* seed. Seed were imbibed for 24 hours in the dark supplemented with KAR_1 and KAR_2. Transcripts were normalised to *BtCACS* reference transcripts. Data are means ± SE, *n* = 3 biological replicates, ≥50 seeds per replicate. **c**, **d**, Hypocotyl elongation responses of *B. tournefortii* seedlings treated with KAR_1 and KAR_2 and grown for four days under continuous red light. Data are means ± 95% CI of *n* = 18 to 24 seedlings. Scale bar: 10 mm. **e**, Levels of *BtDLK2* transcripts in *B. tournefortii* seedlings grown under the same conditions as for d. Data are means ± SE, *n* = 3 biological replicates, ≥20 seedlings per replicate. In all panels, asterisks denote significance levels

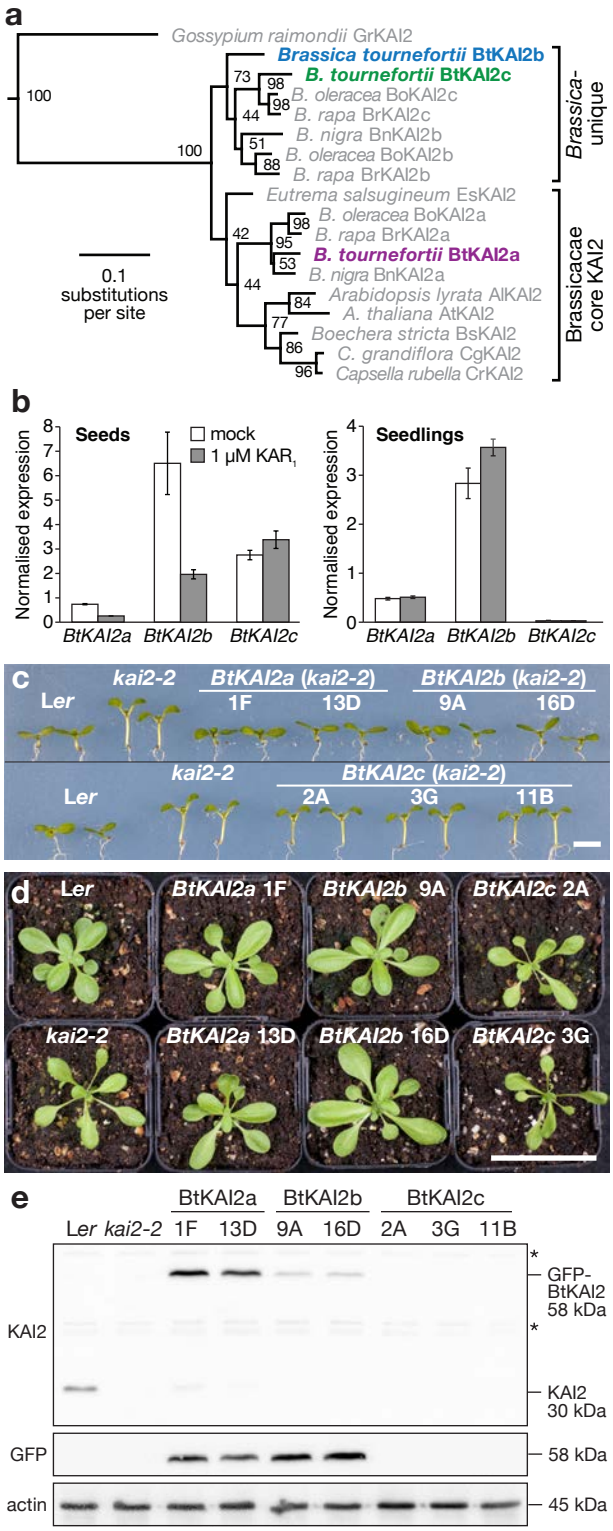

Figure 2. Two differentially expressed *B. tournefortii* KAI2 homologues are functional in Arabidopsis
a, Maximum likelihood phylogeny of KAI2 homologues in the Brassicaceae, based on nucleotide data. Node values represent bootstrap support from 100 replicates. A *KAI2* sequence from *Gossypium raimondii* (Malvaceae) serves as an outgroup. Tree shown is a subset of a larger phylogeny in Supplementary Figure 2. **b**, Transcript levels of the three *BtKAI2* homologues in *B. tournefortii* seed imbibed for 24 h (left) and four-day-old *B. tournefortii* seedlings (right) treated with or without 1 μM KAR_1 for 24 h. Data are means ± SE, n = 3 biological replicates. **c, d,** Seedling and rosette phenotypes of two independent transgenic lines of Arabidopsis homozygous for *KAI2pro:GFP-BtKAI2* transgenes. Scale bars: 5 mm (**c**); 50 mm (**d**).**e**, Immunoblots of soluble proteins challenged with antibodies against KAI2 (upper panel), GFP (middle panel) or actin (lower panel). Non-specific bands are marked with asterisks. Protein was isolated from pools of approximately fifty 7-day-old seedlings.

We performed transgenic complementation of the Arabidopsis *kai2-2* null mutant by expressing each of the three isoforms as a GFP fusion protein driven by the Arabidopsis *KAI2* promoter (*KAI2pro*:*GFP-BtKAI2*). Such fusions of GFP with KAI2 proteins have been used previously to analyse KAI2 activity[14, 36, 37]. Both *BtKAI2a* and *BtKAI2b* complemented the seedling and leaf phenotypes of *kai2-2*, whereas *BtKAI2c* did not, despite being expressed at the transcriptional level (Fig. 2c-d and Supplementary Fig. 5a). We could not detect GFP-BtKAI2c protein in three independent transgenic lines, while GFP-BtKAI2a and GFP-BtKAI2b accumulated at consistent levels when detected using an anti-GFP antibody (thereby negating the effects of sequence differences in the anti-KAI2 epitope region; Fig. 2e and Supplementary Fig. 5b). To rule out the possibility that the *GFP-BtKAI2c* transgene is inaccurately expressed in Arabidopsis, we amplified the full-length cDNA from transgenic plant material by RT-PCR, generating a product of the expected size (Supplementary Fig. 6). Two sequenced clones of this RT-PCR product matched the original coding sequence present in the transgene. As such, the *GFP-BtKAI2c* mRNA is processed faithfully in Arabidopsis, and the apparent absence of protein is most likely a result of posttranslational events. Consistent with this interpretation, transient expression in tobacco leaves produced levels of BtKAI2c protein that were considerably lower than for BtKAI2a and BtKAI2b, suggesting that BtKAI2c is poorly expressed in plant cells (Supplementary Fig. 5c). BtKAI2c carries several unique amino acid substitutions, which together may compromise protein folding and stability (Supplementary Fig. 3). Therefore, we conclude that BtKAI2a and BtKAI2b are functionally orthologous to AtKAI2 in regulating plant development, whereas BtKAI2c is an aberrant gene that is potentially non-functional.

BtKAI2a and BtKAI2b show differential ligand specificity

We further characterised the ligand specificity of *BtKAI2* homologues by performing physiological and molecular assays with the transgenic lines. Primary-dormant Arabidopsis seeds homozygous for the transgenes were tested for germination response (Fig. 3a and Supplementary Fig. 7). Germination of *BtKAI2b* transgenic seeds was more responsive to KAR_1 than KAR_2 at 1 µM, whereas no significant difference was observed for *BtKAI2a* transgenic seeds. *BtKAI2c* transgenic seeds were insensitive to karrikins. Hypocotyl elongation responses (Fig. 3b) and accumulation patterns of *DLK2* transcripts (Fig. 3c) agreed with the germination response with respect to karrikin preferences. Therefore, and consistent with their relative phylogenetic positions (Fig. 2a), we conclude that *BtKAI2a* has similarity to *AtKAI2* in terms of ligand specificity, whereas *BtKAI2b* has a preference for KAR_1 over KAR_2. As *BtKAI2b* is more highly expressed than *BtKAI2a* in *B. tournefortii* seed and seedlings (Fig. 2b), we suggest that

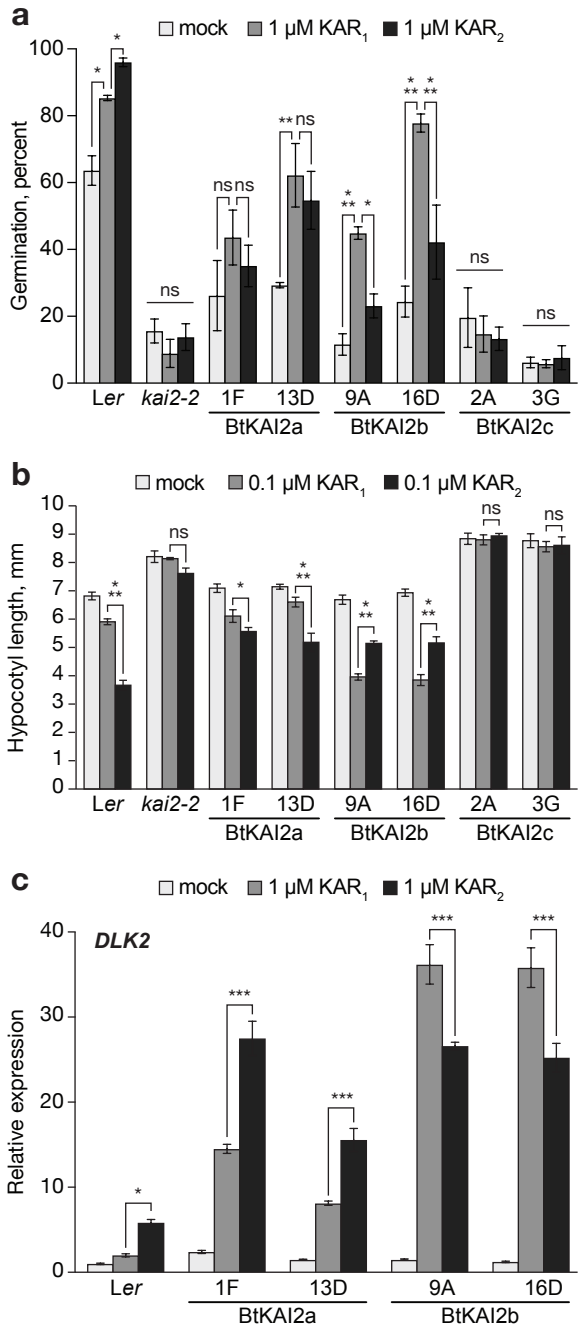

Figure 3. Functional divergence between BtKAI2 homologues

a, Germination responses of primary dormant Arabidopsis seed homozygous for *KAI2pro:GFP-BtKAI2* transgenes in the *kai2-2* background. Germination values were determined 120 h after sowing. Extended germination curves are shown in Supplementary Fig. 6. Data are means ± SE of n = 3 independent seed batches, 75 seed per batch. **b**, Hypocotyl elongation responses of *KAI2pro:GFP-BtKAI2* seedlings treated with KAR_1 or KAR_2. Data are means ± SE of n = 3 biological replicates, 12–18 seedlings per replicate. **c**, Levels of *DLK2* transcripts in 8-day-old *KAI2pro:GFP-BtKAI2* seedlings treated with KAR_1 or KAR_2 for eight hours. Expression was normalised to *CACS* reference transcripts and scaled to the value for mock-treated seedlings within each genotype. Data are means ± SE of n = 3 biological replicates. Pairwise significant differences: * $P < 0.05$ ** $P < 0.01$ *** $P < 0.001$; ns, $P > 0.05$ (two-way ANOVA).

the ligand specificity of BtKAI2b accounts for the enhanced KAR_1-responsiveness of this species.

Positions 98 and 191 account for ligand specificity between BtKAI2a and BtKAI2b

To investigate interactions between BtKAI2 homologues and ligands, we performed differential scanning fluorimetry (DSF) assays on purified recombinant proteins (Supplementary Fig. 8). DSF has been used extensively for inferring the interaction of strigolactone-like compounds with D14- and KAI2-related proteins[25, 37, 38, 39, 40, 41]. Racemic GR24 is a widely-used synthetic strigolactone analogue that consists of two enantiomers, of which GR24$^{ent\text{-}5DS}$ is bioactive via AtKAI2[42]. Catalytically inactive D14 and KAI2 variants do not respond to GR24 in DSF, suggesting that the shift in thermal response results from ligand hydrolysis and a corresponding conformational change in the receptor[25, 37, 39]. In DSF assays, AtKAI2 shows a specific response to >100 µM GR24$^{ent\text{-}5DS}$ but, for unclear reasons, no response to karrikins[37]. Likewise, we found that both BtKAI2a and BtKAI2b were also unresponsive to karrikins in DSF (Supplementary Fig. 9a). Therefore, we used GR24$^{ent\text{-}5DS}$ as a surrogate substrate in DSF assays to interrogate BtKAI2–ligand interactions.

We found that AtKAI2 and BtKAI2a showed similar responses to >100 µM GR24$^{ent\text{-}5DS}$, but the BtKAI2b response was clear at >25 µM (Supplementary Fig. 9b). We then used a lower range of GR24$^{ent\text{-}5DS}$ concentrations (0–50 µM) to determine the threshold for response, which we defined as a statistically significant reduction in the maximal rate of change in fluorescence at the melting temperature of the protein (T_m). Although BtKAI2a showed only a weak and non-significant response at 40 and 50 µM GR24$^{ent\text{-}5DS}$, BtKAI2b responded significantly at 10 µM and above (Fig. 4a). These results suggest that BtKAI2b is more sensitive than BtKAI2a to GR24$^{ent\text{-}5DS}$, and that BtKAI2a is most like AtKAI2 in this respect.

BtKAI2a and BtKAI2b differ in primary amino acid sequence at just 14 positions (Supplementary Fig. 3). We postulated that differences in ligand specificity might be determined by amino acids in the vicinity of the ligand binding pocket. Protein structural homology models revealed only two residues that differ in this region: V98 and V191 in BtKAI2a (Fig. 4b), and L98 and L191 in BtKAI2b (Fig. 4c); the corresponding residues in AtKAI2 (Fig. 4d) and AtD14 (Fig. 4e) are valines. Residue 98 is immediately adjacent to the catalytic serine at the base of the pocket. Residue 191 is located internally on αT4 of the lid domain which, in AtD14, is associated with a major rearrangement of protein structure upon ligand binding that reduces the size of the pocket[27]. Homology modelling suggests only subtle

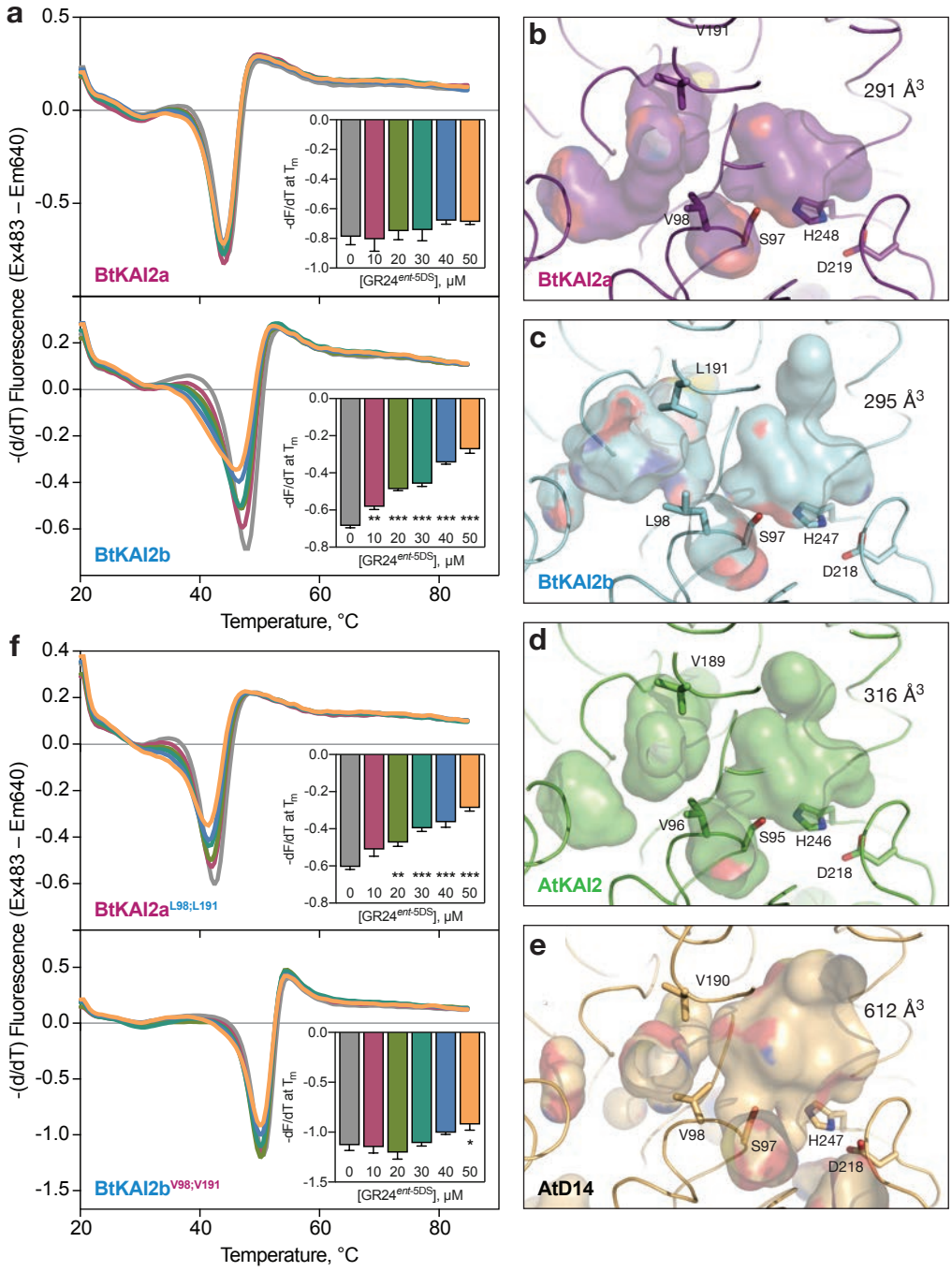

Figure 4. Two residues account for ligand specificity between BtKAI2a and BtKAI2b
a, DSF curves of SUMO-BtKAI2a and SUMO-BtKAI2b fusion proteins treated with 0-50 µM GR24$^{ent\text{-}5DS}$, a KAI2-bioactive ligand. Each curve is the average of three sets of reactions, each comprising four technical replicates. Insets plot the minimum value of –(dF/dT) at the melting point of the protein as determined in the absence of ligand (means ± SE, n = 3). Significant differences from untreated control: * $P < 0.05$ ** $P < 0.01$ *** $P < 0.001$ (ANOVA). **b**, DSF curves of SUMO-BtKAI2a$^{L98;L191}$ and SUMO-BtKAI2b$^{V98;V191}$ fusion proteins treated with 0-50 µM GR24$^{ent\text{-}5DS}$. **c–f**, Solved structure of AtKAI2 (PDB: 3w06, Kagiyama et al 2013), AtD14 (PDB: 4IH4, Zhao et al 2013) and derived homology models of BtKAI2a and BtKAI2b. Coloured surfaces depict internal cavities; values indicate the volumes of the primary ligand-binding cavities, adjacent to the catalytic Ser-His-Asp residues. Also shown is a variable secondary pocket, to the left of the primary pocket in these images.

differences in the size and shape of the primary ligand binding pocket of BtKAI2a and BtKAI2b (Fig. 4b-c). To determine if these residues are pertinent to ligand specificity, we replaced the two valine residues of BtKAI2a with leucine residues, generating the variant BtKAI2a$^{L98;L191}$, and *vice-versa* for BtKAI2b, generating the variant BtKAI2b$^{V98;V191}$ (Supplementary Fig. 8). In DSF assays, we found that exchanging the two residues was sufficient to switch the original responses, such that BtKAI2a$^{L98;L191}$ responded sensitively to GR24$^{ent\text{-}5DS}$, but BtKAI2b$^{V98;V191}$ did not (Fig. 4f).

We reasoned that the most robust method to assess the effect of residues 98 and 191 upon the response to karrikins was to test their function directly *in planta*. We expressed BtKAI2a$^{L98;L191}$ and BtKAI2b$^{V98;V191}$ in the Arabidopsis *kai2-2* null mutant background, and selected two independent homozygous transgenic lines for each, on the basis of protein expression level and segregation ratio (Supplementary Fig. 10). Using two different assays, we found that substitutions between BtKAI2a and BtKAI2b at positions 98 and 191 also reversed karrikin preference in Arabidopsis seedlings (Fig. 5a-b; Supplementary Fig. 11). Most prominently, the clear preference of BtKAI2b for KAR_1 was unambiguously reversed to a preference for KAR_2 in *GFP-BtKAI2b$^{V98;V191}$* transgenics, effectively recapitulating the response of the native BtKAI2a protein. Taken together, these results demonstrate that these two variant residues are sufficient to account for differences in ligand specificity between BtKAI2a and BtKAI2b. Finally, given the importance of these residues, it is notable that the non-functional BtKAI2c carries a highly non-conservative arginine residue at position 98, which might disrupt ligand binding, if not protein folding entirely (Supplementary Fig. 3).

DISCUSSION

The KAI2–D14 family of α/β-hydrolases is characterised by reactivity towards butenolide compounds, including endogenous strigolactones and strigolactone-related compounds, abiotic karrikins derived from burnt vegetation, and synthetic strigolactone analogues with a wide array of functional groups. Direct evidence for a receptor-ligand relationship between karrikins and KAI2 homologues stems from crystallography and *in vitro* binding assays. Two crystal structures of KAR-responsive KAI2 proteins from Arabidopsis and the parasitic plant *Striga hermonthica* reveal largely similar overall protein structure, but surprisingly are non-congruent with respect to KAR_1 binding position and orientation[43, 44]. The affinity of AtKAI2 for KAR_1 is imprecisely defined, with estimates of dissociation coefficients (Kd) ranging from 4.6

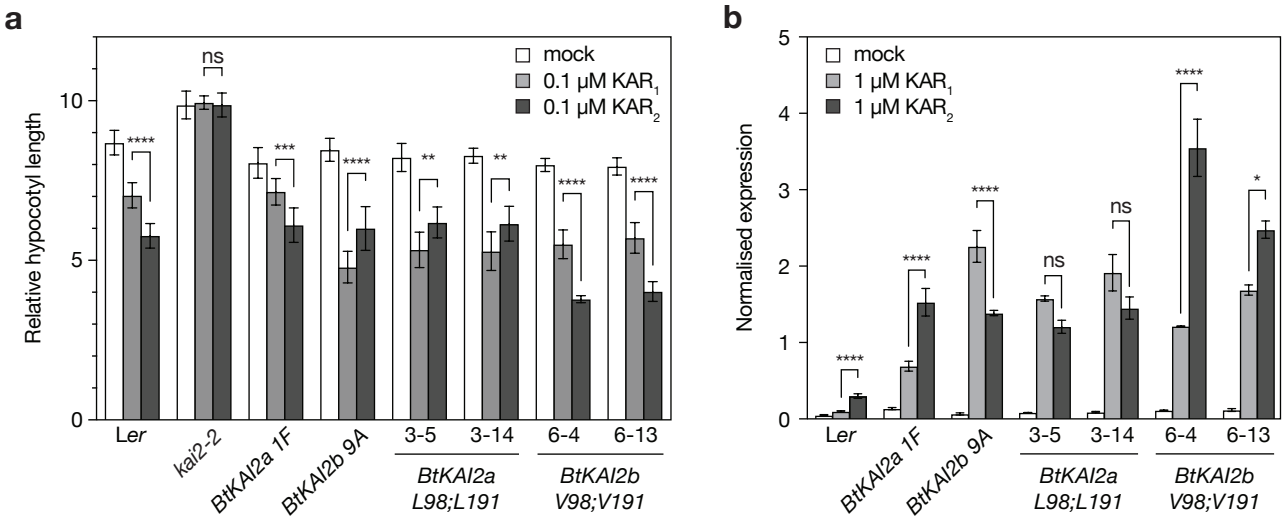

Figure 5. Substitutions between BtKAI2a and BtKAI2b at positions 98 and 191 reverse karrikin preference in transgenic Arabidopsis.

a, Hypocotyl elongation responses to karrikins in two independent transgenic lines homozygous for *GFP-BtKAI2a*$^{L98;L191}$ (3-5, 3-14) and two lines for *GFP-BtKAI2b*$^{V98;V191}$ (6-4, 6-13). Data shown are a summary of three experimental replicates performed on separate occasions, each comprising 20-40 seedlings per genotype/treatment combination. Data for each replicate are shown in Supplementary Figure 10. Error bars are SE, n=3 experimental replicates; each dot corresponds to the mean value derived from each replicate. Asterisks denote significant differences: * P<0.05, ** P<0.01, *** P<0.001, **** P<0.0001 (linear mixed model with experimental replicate as a random effect; specific pairwise comparisons using Tukey's HSD correction).

b, Levels of *DLK2* transcripts in the same transgenic lines treated with 1 μM KAR_1, 1 μM KAR_2, or 0.1% acetone and harvested 8 hours later. Expression was normalised to *CACS* reference transcripts. Data are means ± SE of n=3 pools of 50-100 seedlings treated in parallel. Asterisks denote significant differences as above (two-way ANOVA; specific pairwise comparisons using Tukey's HSD correction).

μM[45], to 26 μM[46], to 148 μM[47] using isothermal calorimetry, and 9 μM using fluorescence microdialysis[43]. While variability in affinity estimates can be explained in part by different experimental conditions and techniques, it should also be considered that, depending on the homologue under examination, KAR_1 may not be the optimal ligand. Our data, which benefit from clear and distinct biological responses, provide strong evidence that KAI2 is sufficient to determine ligand specificity, which in turn strengthens the case that KAI2 is the receptor by which karrikins are perceived.

Ligand specificity is a key contributor to functional distinction between KAI2–D14 family receptors, and elucidating the molecular mechanisms behind ligand specificity is a significant research challenge. In certain root-parasitic weeds in the Orobanchaceae, substitutions of bulky residues found in AtKAI2 with smaller hydrophobic amino acids that increase the ligand-binding pocket size have likely improved the affinity for host-derived strigolactone ligands, as opposed to the smaller-sized karrikin ligands[48, 49, 50]. Moreover, lid-loop residues that affect the rigidity and size of the ligand entry tunnel determine the ligand selectivity between KAR_1 and *ent*-5-deoxystrigol (a strigolactone analogue with non-natural stereochemistry) among eleven KAI2 homologues in *Physcomitrella patens*[51]. Karrikin and strigolactone compounds also show chemical diversity within themselves, yet ligand discrimination among KAI2–D14 family receptors is not well characterised. Our data demonstrate that, in the case of BtKAI2 proteins, different KAI2 homologues respond differently to highly similar KAR analogues, and that subtle changes in pocket residues likely account for preferences between these ligands. Although the identified residues L98 and L191 do not significantly change the pocket size of BtKAI2b in comparison to BtKAI2a, these residues would make the BtKAI2b pocket more hydrophobic, which is consistent with KAR_1 being more hydrophobic than KAR_2[4]. Therefore, ligand specificity between highly-similar chemical analogues can be achieved through fine-tuning of pocket hydrophobicity. Similarly subtle changes have been reported for the rice gibberellin receptor GID1: changing Ile133 to Leu or Val increases the affinity for GA_{34} relative to the less polar GA_4, which lacks just one hydroxyl group[52]. KAI2–D14 family receptors may also show ligand specificity towards diverse natural strigolactones, resulting in part from multiplicity of biosynthetic enzymes, such as the cytochrome P450 enzymes in the MAX1 family[38, 53, 54] and supplementary enzymes such as LATERAL BRANCHING OXIDOREDUCTASE[55]. Although the functional reasons underlying such strigolactone diversity are still unclear, it is possible that variation among D14 homologues yields varying affinities for different strigolactone analogues[56]. As an increasingly refined picture emerges of the features that determine ligand

specificity for KAI2–D14 family receptors, we envision the rational design of synthetic receptor proteins with desirable ligand specificity in the future.

Gene duplication is a common feature in plant evolutionary histories as an initial step towards neofunctionalisation[57]. In obligate parasitic weeds, duplication and diversification of *KAI2* genes (also referred to as *HTL* genes) have shifted ligand specificity towards strigolactones[48, 49]. Karrikins, as abiotic molecules with limited natural occurrence, are unlikely to be the natural ligand for most KAI2 proteins, which are found throughout land plants. Instead, the evolutionary maintenance of a highly conserved receptor probably reflects the core KAI2 function of perceiving an endogenous ligand ("KL") that regulates plant development[30, 31, 32]. This core function is presumably retained after gene duplication events through ancestral, non-divergent copies that are under purifying selection[48, 49]. KAI2 diversity may also reflect differing affinity for KL analogues in different species and at different life stages. Our results are consistent with a scenario in which both BtKAI2a and BtKAI2b have retained the core KAI2 function of perceiving KL to support plant development, because both copies fully complement the Arabidopsis *kai2* phenotype. However, BtKAI2b has also acquired mutations that alter its ligand specificity, which in turn enhance sensitivity to the more abundant karrikin released after fire. The *BtKAI2b* gene is also more highly expressed than *BtKAI2a* in seeds and seedlings, consistent with an adaptation to post-fire seedling establishment. This diversity among KAI2 proteins may provide *B. tournefortii* with a selective advantage in fire-prone environments, assisting its invasive nature.

Recent findings indicate that KAI2 is an integrator that also modulates germination in response to other abiotic environmental signals, including temperature and salinity[58]. As seed germination is a critical life stage that contributes to the invasiveness of a species, strategies for weed control will benefit from specific knowledge of KAI2 sequence diversity and expression profiles.

METHODS

Chemical synthesis

Karrikins (KAR_1 and KAR_2), $^{13}[C]_5$-labelled karrikins and GR24 enantiomers ($GR24^{5DS}$ and $GR24^{ent\text{-}5DS}$) were prepared as previously described[59, 60].

Plant material

Arabidopsis *kai2-2* (L*er*) and *Atd14-1* (Col-0) mutants were previously described[15]. Arabidopsis plants were grown on a 6:1:1 mixture of peat-based compost (Seedling Substrate Plus; Bord Na Mona, Newbridge, Ireland), vermiculite and perlite, respectively. Light was provided by wide-spectrum white LED panels emitting 120-150 µmol photons.m^{-2}.s^{-1} with a 16 h light/8 h dark photoperiod, a 22 °C light/16 °C dark temperature cycle, and constant 60% relative humidity. The seeds of *Brassica tournefortii* used in this work were collected in November and December 2009 from two sites in Western Australia (Kings Park in Perth, and Merridin)[61]. *Brassica tournefortii* seeds were dried to 15% relative humidity for one month prior to storage in air-tight bags at –20 °C.

Seed germination assays

Seed germination assays using Arabidopsis were performed on Phytagel as described previously[42]. *Brassica tournefortii* seeds were sowed in triplicates (35-70 seeds each) on glass microfibre filter paper (Grade 393; Filtech, NSW Australia) held in petri dishes and supplemented with mock or karrikin treatments. Treatments were prepared by diluting acetone (mock) or karrikin stocks (dissolved in acetone) 1:1000 with ultrapure water. Because germination of *B. tournefortii* is inhibited by light[8], the seeds were imbibed in the dark at 22 °C. Numbers of germinated seeds were counted each day until the germination percentages remained unchanged.

Hypocotyl elongation assays

Arabidopsis hypocotyl elongation assays were performed under red light as described previously[15]. For *B. tournefortii*, assays were performed with the following modifications to the Arabidopsis protocol: *B. tournefortii* seeds were sowed in triplicate on glass microfibre filter paper (Filtech) held in petri-dishes supplemented with mock or karrikin treatments. The seeds were imbibed in the dark for 22 h at 24 °C before exposing to continuous red light (5 µmol photons m^{-2} s^{-1}) for 4 days.

Transcript analysis

Brassica tournefortii seeds were imbibed on glass fibre filters in the dark at 22 °C as described above. For transcript quantification in *B. tournefortii* seeds, samples were taken at the indicated time points, briefly blot-dried on paper towel, and frozen in liquid nitrogen. For *B. tournefortii*

seedlings, two methods were used. For data shown in Fig. 1e, seeds were sowed and seedlings grown in triplicate under identical conditions to those described for hypocotyl elongation assays For data shown in Fig. 2b, seeds were first imbibed for 24 h in the dark, and then transferred to the growth room (~120-150 µmol photons m^{-2} s^{-2} white light, 16 h light/8 h dark, 22 °C light/16 °C dark) for three days. A sample of approximately 20 seedlings was then transferred to a 250 mL conical flask containing 50 mL sterile ultrapure water supplemented with 1 µM KAR_1, or an equivalent volume of acetone (0.1% v/v), with three replicate samples per treatment. The flasks were then shaken for 24 h before seedlings were harvested.

Arabidopsis seedlings were grown on 0.5× MS agar under growth room conditions (wide-spectrum white LED panels emitting 120-150 µmol photons.m^{-2}.s^{-1} with a 16 h light/8 h dark photoperiod and a 22 °C light/16 °C dark temperature cycle) for seven days. On the seventh day, seedlings were transferred to 3 mL liquid 0.5× MS medium in 12-well culture plates (CORNING Costar 3513) and shaken at 70 rpm for a further 22 h under the same growth room conditions. The medium was then removed by pipette and replaced with fresh medium containing relevant compounds or an equivalent volume (0.1% v/v) acetone. After a further incubation period with shaking (8 h), the seedlings were harvested, blotted dry, and frozen in liquid nitrogen.

RNA extraction, DNase treatment, cDNA synthesis and quantitative PCR were conducted as previously described[62]. All oligonucleotides are listed in the Supplementary Table 2.

Cloning and mutagenesis of *Brassica tournefortii KAI2* and *D14* homologues

Full-length *BtKAI2* coding sequences (and unique 3′UTR sequences) were amplified from *B. tournefortii* cDNA with Gateway-compatible *attB* sites using the universal forward primer BtKAI2_universal_F and homologue-specific reverse primers RACE_R (BtKAI2a), Contig1_R (BtKAI2b) and Contig5_R (BtKAI2c), before cloning into pDONR207 (Life Technologies). The pDONR207 clones were confirmed by Sanger sequencing and recombined with pKAI2pro-GFP-GW[37] to generate the binary plant expression plasmids pKAI2pro-GFP-BtKAI2a, pKAI2pro-GFP-BtKAI2b and pKAI2pro-GFP-BtKAI2c. For transient expression in tobacco, BtKAI2 coding sequences were transferred via Gateway-mediated recombination into pSKI106, which drives very high expression and encodes an N-terminal 3× *c*-myc tag[63]. The *BtD14a* coding sequence was amplified from cDNA using oligonucleotides BtD14_F and BtD14_R, cloned into pDONR207 as above, and transferred into pD14pro-GW[37].

The full-length *BtKAI2* coding sequences (excluding 3′UTRs) were amplified from the pDONR207 clones and reconstituted with the pE-SUMO vector by Gibson Assembly to generate the heterologous expression plasmids pE-SUMO-BtKAI2a and pE-SUMO-BtKAI2b. Site-directed mutagenesis generated the heterologous expression plasmids pE-SUMO-BtKAI2a$^{L98;L191}$ and pE-SUMO-BtKAI2b$^{V98;V191}$. For expression of *GFP-BtKAI2a*$^{L98;L191}$ and *GFP-BtKAI2b*$^{V98;V191}$ variants in Arabidopsis, site-directed mutagenesis was performed on pDONR207 clones prior to recombination with pKAI2pro-GFP-GW. In both cases, the targeted residues were mutated simultaneously in one PCR product, while the remainder of the plasmid was amplified in a second PCR product. The mutated plasmids were reconstituted by Gibson assembly, and coding regions confirmed by Sanger sequencing.

Plant transformation

Homozygous *kai2-2* plants were transformed by floral dip. Primary transgenic seedlings were selected on sterile 0.5× MS medium supplemented with 20 µg/mL hygromycin B. T_2 lines exhibiting a 3:1 ratio of hygromycin resistant-to-sensitive seedlings were propagated further to identify homozygous lines in the T_3 generation. Experiments were performed from the T_3 generation onwards.

For transient expression in tobacco, *Agrobacterium* (GV3101) carrying pSKI106 variants was grown in LB medium (25 mL) supplemented with antibiotics and 20 µM acetosyringone until OD_{600} reached 1.0. The bacteria were then harvested by centrifugation (15 min, 5000 × *g*) and resuspended in 10 mM $MgCl_2$, 10 mM MES (pH 5.6) and 100 µM acetosyringone. The optical density was adjusted to 0.4, and the suspension was left standing at 22 °C overnight (approximately 14 h). Leaves of three-week-old *Nicotiana benthamiana* were then infiltrated with a 5-mL syringe, through the abaxial leaf surface. After four days, the leaves were collected and frozen in liquid nitrogen.

Karrikin uptake measurements

Fifteen samples of seed were sowed for each karrikin treatment (five time points, each in triplicate). In each sample, approximately 40 mg of *Brassica tournefortii* seeds were imbibed in 3 mL ultrapure water for 24 h in 5-mL tubes. After centrifugation (2 min at 3220 × *g*), excess water was removed by pipette and the volume of residual water (mostly absorbed into the seeds) was calculated by weighing the seeds before and after imbibition. Fresh ultrapure water was added to the fully-imbibed seeds to reach a total volume of 980 µL. Then 20 µL of 100 µM

KAR_1 or KAR_2 was added to a final concentration of 2 µM. The seeds were imbibed at 22 °C in darkness. At the indicated time point (0, 2, 4, 8 or 24 h post-treatment), 500 µL of the imbibition solution was removed and combined with 100 ng of either $^{13}[C]_5$-KAR_1 or $^{13}[C]_5$-KAR_2 (100 µL at 1 µg/mL) as an internal standard for quantification purposes. The sample was then extracted once with ethyl acetate (500 µL), and 1 µL of this organic layer was analysed using GC-MS in selective ion monitoring (SIM) mode as previously described[64].

The amount of KAR_1 in each sample was calculated by the formula $\frac{A(Ion150)}{A(Ion155)}$×100 ng and converted to moles, where *A(Ion150)* indicates the peak area of the ion 150 (KAR_1 to be measured), *A(Ion151)* indicates the peak area of the ion 151 ($^{13}[C]_5$-KAR_1), and 100 ng is the amount of $^{13}[C]_5$-KAR_1 spiked in before the ethyl acetate extraction. Similarly, the amount of KAR_2 in each sample was calculated by the formula $\frac{A(Ion136)}{A(Ion141)}$×100 ng and converted to moles. The uptake percentage adjusted to 40 mg of *B. tournefortii* seeds was calculated by the formula: $(1 - \frac{N(x)}{N(0)}) \times \frac{40\ mg}{m\ (seed)}$, where N(0) indicates moles of karrikins at time 0, $N(x)$ indicates moles of karrikins at time point *x*, and $m(seed)$ indicates the dry weight (mg) of seeds tested in each replicate. For Arabidopsis seeds, the procedure was scaled down for a smaller mass of seeds (20 mg).

Transcriptome assembly and analysis

Twenty milligrams of dry *B. tournefortii* seed was imbibed in water for 24 h and incubated at 22 °C in the dark. The seeds were collected by centrifugation, blotted dry, and frozen in liquid nitrogen. A separate sample of seed was sown on glass filter paper, imbibed for 24 h as above, and then incubated for 96 h under continuous red light (20 µmol m^{-2} s^{-1}) with a 22 °C (16 h)/16 °C (8h) temperature cycle. A single sample of seedlings (50 mg fresh weight) was harvested and frozen in liquid nitrogen. Total RNA was extracted from both seed and seedling samples using the Spectrum Plant RNA kit (Sigma-Aldrich), including an on-column DNase step. $PolyA^+$ mRNA was purified using oligo(dT) magnetic beads (Illumina), and cDNA libraries for sequencing were generated as described[65]. Sequencing was performed on the Illumina HiSeq 2000 platform at the Beijing Genomic Institute, Shenzhen, China. Raw reads were filtered to remove adapters and low-quality reads (those with >5% unknown nucleotides, or those in which greater than 20% of base calls had quality scores ≤10). After filtering, both libraries generated reads with >99.9% of nucleotides attaining Q20 quality score. Transcriptome *de novo* assembly was performed with Trinity[66]. For each library, contigs were assembled into Unigenes;

Unigenes from both libraries were then combined, yielding a total of 45,553 predicted coding region sequences with a mean length of 1011 nt. The combined Unigenes were then interrogated for homology to *AtKAI2*, *AtD14*, *AtDLK2*, *AtSTH7* and *AtCACS* using BLASTn searches.

Phylogenetic analysis

KAI2 and *D14* homologues in *Brassica* species were identified from BLAST searches using Arabidopsis coding sequences as a query. Additional sequences were sampled from an extended phylogenetic analysis[29]. Multiple sequence alignments were performed using MAFFT plugin implemented in Geneious R10 (Biomatters). The alignment was trimmed slightly at the 5′ end to remove non-aligned regions of monocot D14 sequences. Maximum likelihood phylogenies were generated using PHYML (GTR +G +I substitution model, combination of NNI and SPR search, and 100 bootstraps). The choice of substitution model was guided by Smart Model Selection in PhyML[67] (http://www.atgc-montpellier.fr/sms). A list of all sequences, and their sources, is provided in Supplementary Table 1.

Protein homology modelling

KAI2 structures were modelled using the SWISS-MODEL server (https://swissmodel.expasy.org) using the alignment mode[68] and the *Arabidopsis thaliana* KAI2 structure 3w06 as a template[45]. Figures of protein structure and homology models were generated using PyMOL v1.3 (Schrödinger LLC). Cavity surfaces were visualised using the "cavities & pockets (culled)" setting in PyMOL and a cavity detection cut-off value of four solvent radii. Cavity volumes were calculated using the CASTp server v3.0[69] (http://sts.bioe.uic.edu/castp) with a probe radius of 1.4Å. Values indicate Connolly's solvent-excluded volumes. Cavities were inspected visually using Chimera v1.12 (https://www.cgl.ucsf.edu/chimera/). For both BtKAI2a and BtKAI2b models, CASTp erroneously included surface residues near the primary pocket entrance in the calculation of the pocket volumes. This issue was resolved by the artificial placement of a free alanine residue adjacent to the cavity entrance, as described previously[70].

Protein expression and purification

BtKAI2 proteins were generated as N-terminal 6×HIS-SUMO fusion proteins. All proteins were expressed in BL21 Rosetta DE3 pLysS cells (Novagen) and purified using IMAC as described in detail previously[37].

Differential scanning fluorimetry

DSF was performed in 384-well format and thermal shifts were quantified as described previously[37]. Reactions (10 µL) contained 20 µM protein, 20 mM HEPES pH 7.5, 150 mM NaCl, 1.25% (v/v) glycerol, 5× SYPRO Tangerine dye (Molecular Probes) and varying concentrations of ligand that resulted in a final concentration of 5% (v/v) acetone.

Statistical analysis

Data were analysed using one- or two-way ANOVA (α = 0.05, with Tukey's multiple comparisons test). For Figure 5a, in which data from three experimental replicates were combined, data were analysed using a mixed effects model with experimental replicate as a random effect, and genotype and treatment as fixed effects. Prior to ANOVA, germination data were arcsine-transformed, and gene expression data were log-transformed. Tests were implemented in GraphPad Prism version 7.0 or 8.0 (GraphPad Software, graphpad.com).

Sequence data

Sequence data are available at NCBI Genbank under the following accessions: *BtKAI2a*, MG783328; *BtKAI2b*, MG783329; *BtKAI2c*, MG783330; *BtD14a*, MG783331; *BtD14b*, MG783332; *BtDLK2*, MG783333; *BtSTH7*, MK756121; *BtCACS*, MK756122. Raw RNA sequence data from *Brassica tournefortii* seed and seedlings are available in the NCBI SRA database under accession SRP128835.

REFERENCES

1. Early R, *et al.* Global threats from invasive alien species in the twenty-first century and national response capacities. *Nat Commun* **7**, 12485-12485 (2016).

2. Flematti GR, *et al.* Karrikin and cyanohydrin smoke signals provide clues to new endogenous plant signaling compounds. *Molecular Plant* **6**, 29-37 (2013).

3. Keeley JE, Pausas JG. Evolution of 'smoke' induced seed germination in pyroendemic plants. *South African Journal of Botany* **115**, 251-255 (2018).

4. Flematti GR, Ghisalberti EL, Dixon KW, Trengove RD. Identification of Alkyl Substituted 2 H-Furo[2,3- c]pyran-2-ones as Germination Stimulants Present in Smoke. *Journal of Agricultural and Food Chemistry* **57**, 9475-9480 (2009).

5. Long RL, Stevens JC, Griffiths EM, Adamek M, Powles SB, Merritt DJ. Detecting karrikinolide responses in seeds of the Poaceae. *Australian Journal of Botany* **59**, 610-620 (2011).

6. Milberg P, Lamont BB. Fire enhances weed invasion of roadside vegetation in southwestern Australia. *Biological Conservation* **73**, 45-49 (1995).

7. Bangle DN, Walker LR, Powell EA. Seed germination of the invasive plant *Brassica tournefortii* (Sahara mustard) in the Mojave Desert. In: *Western North American Naturalist* **68**, 334-342 (2008).

8. Long RL*, et al.* Seeds of Brassicaceae weeds have an inherent or inducible response to the germination stimulant karrikinolide. *Annals of Botany* **108**, 933-944 (2011).

9. Brooks ML*, et al.* Effects of Invasive Alien Plants on Fire Regimes. *BioScience* **54**, 677 (2004).

10. Sanders R, Minnich R. Brassica tournefortii. In: *Invasive Plants of California's Wildlands* (eds Bossard CC, Randall JM, Hoshovsky MC). University of California Press (2000).

11. Stevens J, Merritt D, Flematti G, Ghisalberti E, Dixon K. Seed germination of agricultural weeds is promoted by the butenolide 3-methyl-2H-furo[2,3-c]pyran-2-one under laboratory and field conditions. *Plant Soil* **298**, 113-124 (2007).

12. Schiermeier Q. Pall hangs over desert's future as alien weeds fuel wildfires. *Nature* **435**, 724 (2005).

13. Steers RJ. Invasive Plants, Fire Succession, and Restoration of Creosote Bush Scrub in Southern California. UNIVERSITY OF CALIFORNIA RIVERSIDE (2008).

14. Sun X-D, Ni M. HYPOSENSITIVE TO LIGHT, an Alpha/Beta Fold Protein, Acts Downstream of ELONGATED HYPOCOTYL 5 to Regulate Seedling De-Etiolation. *Molecular Plant* **4**, 116-126 (2011).

15. Waters MT, *et al.* Specialisation within the DWARF14 protein family confers distinct responses to karrikins and strigolactones in Arabidopsis. *Development* **139**, 1285-1295 (2012).

16. Durvasula A, *et al.* African genomes illuminate the early history and transition to selfing in *Arabidopsis thaliana*. *Proceedings of the National Academy of Sciences* **114**, 5213-5218 (2017).

17. Nelson DC, *et al.* Karrikins discovered in smoke trigger Arabidopsis seed germination by a mechanism requiring gibberellic acid synthesis and light. *Plant Physiology* **149**, 863-873 (2009).

18. Flematti GR, Goddard-Borger ED, Merritt DJ, Ghisalberti EL, Dixon KW, Trengove RD. Preparation of 2H-furo[2,3-c]pyran-2-one derivatives and evaluation of their germination-promoting activity. *Journal of Agricultural and Food Chemistry* **55**, 2189-2194 (2007).

19. Flematti GR, Ghisalberti EL, Dixon KW, Trengove RD. A compound from smoke that promotes seed germination. *Science* **305**, 977 (2004).

20. Waters MT, Gutjahr C, Bennett T, Nelson DC. Strigolactone Signaling and Evolution. *Annual Review of Plant Biology* **68**, 291-322 (2017).

21. Yao R, Chen L, Xie D. Irreversible strigolactone recognition: a non-canonical mechanism for hormone perception. *Current Opinion in Plant Biology* **45**, 155-161 (2018).

22. Scaffidi A, *et al.* Exploring the molecular mechanism of karrikins and strigolactones. *Bioorganic & Medicinal Chemistry* **22**, 3743-3746 (2012).

23. Zwanenburg B, Pospíšil T. Structure and Activity of Strigolactones: New Plant Hormones with a Rich Future. *Molecular Plant* **6**, 38-62 (2013).

24. de Saint Germain A, *et al.* An histidine covalent receptor and butenolide complex mediates strigolactone perception. *Nature Chemical Biology* **12**, 787-794 (2016).

25. Seto Y, *et al.* Strigolactone perception and deactivation by a hydrolase receptor DWARF14. *Nat Commun* **10**, 191 (2019).

26. Shabek N, Ticchiarelli F, Mao H, Hinds TR, Leyser O, Zheng N. Structural plasticity of D3–D14 ubiquitin ligase in strigolactone signalling. *Nature* **563**, 652-656 (2018).

27. Yao R, *et al.* DWARF14 is a non-canonical hormone receptor for strigolactone. *Nature* **536**, 469-473 (2016).

28. Marzec M, Brewer P. Binding or Hydrolysis? How Does the Strigolactone Receptor Work? *Trends in Plant Science*, 10.1016/j.tplants.2019.1005.1001 (2019).

29. Bythell-Douglas R, *et al.* Evolution of strigolactone receptors by gradual neo-functionalization of KAI2 paralogues. *BMC Biology* **15**, 52 (2017).

30. Conn CE, Nelson DC. Evidence that KARRIKIN-INSENSITIVE2 (KAI2) Receptors may Perceive an Unknown Signal that is not Karrikin or Strigolactone. *Frontiers in Plant Science* **6**, 1219 (2015).

31. Li W, *et al.* The karrikin receptor KAI2 promotes drought resistance in *Arabidopsis thaliana*. *PLoS Genetics* **13**, e1007076 (2017).

32. Sun YK, Flematti GR, Smith SM, Waters MT. Reporter Gene-Facilitated Detection of Compounds in Arabidopsis Leaf Extracts that Activate the Karrikin Signaling Pathway. *Frontiers in Plant Science* **7**, 1799 (2016).

33. Liu S, *et al.* The *Brassica oleracea* genome reveals the asymmetrical evolution of polyploid genomes. *Nat Commun* **5**, 3930 (2014).

34. Lysak MA, Koch MA, Pecinka A, Schubert I. Chromosome triplication found across the tribe Brassiceae. *Genome Res* **15**, 516-525 (2005).

35. Wang X, *et al.* The genome of the mesopolyploid crop species Brassica rapa. *Nature Genetics* **43**, 1035-1039 (2011).

36. Waters MT, Scaffidi A, Flematti G, Smith SM. Substrate-Induced Degradation of the α/β-Fold Hydrolase KARRIKIN INSENSITIVE2 Requires a Functional Catalytic Triad but Is Independent of MAX2. *Molecular Plant* **8**, 814-817 (2015).

37. Waters MT, Scaffidi A, Moulin SLY, Sun YK, Flematti GR, Smith SM. A *Selaginella moellendorffii* Ortholog of KARRIKIN INSENSITIVE2 Functions in Arabidopsis Development but Cannot Mediate Responses to Karrikins or Strigolactones. *Plant Cell* **27**, 1925-1944 (2015).

38. Abe S, *et al.* Carlactone is converted to carlactonoic acid by MAX1 in Arabidopsis and its methyl ester can directly interact with AtD14 in vitro. *Proceedings of the National Academy of Sciences of the United States of America* **111**, 18084-18089 (2014).

39. Hamiaux C, *et al.* DAD2 Is an α/β Hydrolase Likely to Be Involved in the Perception of the Plant Branching Hormone, Strigolactone. *Current Biology* **22**, 2032-2036 (2012).

40. Hamiaux C, *et al.* Inhibition of strigolactone receptors by N-phenylanthranilic acid derivatives: structural and functional insights. *Journal of Biological Chemistry*, (2018).

41. Végh A, *et al.* Comprehensive Analysis of DWARF14-LIKE2 (DLK2) Reveals Its Functional Divergence from Strigolactone-Related Paralogs. *Frontiers in Plant Science* **8**, (2017).

42. Scaffidi A, *et al.* Strigolactone hormones and their stereoisomers signal through two related receptor proteins to induce different physiological responses in Arabidopsis. *Plant Physiology* **165**, 1221-1232 (2014).

43. Guo Y, Zheng Z, La Clair JJ, Chory J, Noel JP. Smoke-derived karrikin perception by the α/β-hydrolase KAI2 from Arabidopsis. *Proceedings of the National Academy of Sciences of the United States of America* **110**, 8284-8289 (2013).

44. Xu Y, *et al.* Structural basis of unique ligand specificity of KAI2-like protein from parasitic weed Striga hermonthica. *Scientific Reports* **6**, 31386 (2016).

45. Kagiyama M, *et al.* Structures of D14 and D14L in the strigolactone and karrikin signaling pathways. *Genes to Cells* **18**, 147-160 (2013).

46. Toh S, Holbrook-Smith D, Stokes ME, Tsuchiya Y, McCourt P. Detection of parasitic plant suicide germination compounds using a high-throughput Arabidopsis HTL/KAI2 strigolactone perception system. *Chem Commun* **21**, 988-998 (2014).

47. Lee I, *et al.* A missense allele of KARRIKIN-INSENSITIVE2 impairs ligand-binding and downstream signaling in Arabidopsis thaliana. *Journal of Experimental Botany* **69**, 3609-3623 (2018).

48. Conn CE, *et al.* Convergent evolution of strigolactone perception enabled host detection in parasitic plants. *Science* **349**, 540-543 (2015).

49. Toh S, *et al.* Structure-function analysis identifies highly sensitive strigolactone receptors in Striga. *Science* **350**, 203-207 (2015).

50. Xu Y, *et al.* Structural analysis of HTL and D14 proteins reveals the basis for ligand selectivity in Striga. *Nat Commun* **9**, 3947 (2018).

51. Bürger M, *et al.* Structural Basis of Karrikin and Non-natural Strigolactone Perception in Physcomitrella patens. *Cell Reports* **26**, 855-865.e855 (2019).

52. Shimada A, *et al.* Structural basis for gibberellin recognition by its receptor GID1. *Nature* **456**, 520 (2008).

53. Zhang Y, *et al.* Rice cytochrome P450 MAX1 homologs catalyze distinct steps in strigolactone biosynthesis. *Nature Chemical Biology* **10**, 1028-1033 (2014).

54. Challis RJ, Hepworth J, Mouchel C, Waites R, Leyser O. A Role for MORE AXILLARY GROWTH1 (MAX1) in Evolutionary Diversity in Strigolactone Signaling Upstream of MAX2. *Plant Physiology* **161**, 1885-1902 (2013).

55. Brewer PB, *et al. LATERAL BRANCHING OXIDOREDUCTASE* acts in the final stages of strigolactone biosynthesis in *Arabidopsis*. *Proceedings of the National Academy of Sciences* **113**, 6301-6306 (2016).

56. Yoneyama K, *et al.* Which are the major players, canonical or non-canonical strigolactones? *Journal of Experimental Botany* **69**, 2231-2239 (2018).

57. Panchy N, Lehti-Shiu MD, Shiu S-H. Evolution of gene duplication in plants. *Plant Physiology* **171**, 2294-2316 (2016).

58. Wang L, Waters MT, Smith SM. Karrikin-KAI2 signalling provides Arabidopsis seeds with tolerance to abiotic stress and inhibits germination under conditions unfavourable for seedling establishment. *New Phytologist* **219**, 605-618 (2018).

59. Goddard-Borger ED, Ghisalberti EL, Stick RV. Synthesis of the germination stimulant 3-methyl-2H-furo[2,3-c]pyran-2-one and analogous compounds from carbohydrates. *European Journal of Organic Chemistry*, 3925-3934 (2007).

60. Mangnus E, Vanvliet LA, Vadenput D, Zwanenburg B. Structural modifications of strigol analogs - influence of the B and C rings on the bioactivity of the germination stimulant GR24. *Journal of Agricultural and Food Chemistry* **40**, 1222-1229 (1992).

61. Gorecki MJ, Long RL, Flematti GR, Stevens JC. Parental environment changes the dormancy state and karrikinolide response of Brassica tournefortii seeds. *Annals of Botany*, (2012).

62. Waters MT, Smith SM. KAI2- and MAX2-mediated responses to karrikins and strigolactones are largely independent of HY5 in Arabidopsis seedlings. *Molecular Plant* **6**, 63-75 (2013).

63. Kagale S*, et al.* TMV-Gate vectors: gateway compatible tobacco mosaic virus based expression vectors for functional analysis of proteins. *Scientific Reports* **2**, 874 (2012).

64. Flematti GR, Scaffidi A, Dixon KW, Smith SM, Ghisalberti EL. Production of the seed germination stimulant karrikinolide from combustion of simple carbohydrates. *Journal of Agricultural and Food Chemistry* **59**, 1195-1198 (2011).

65. Liang C, Liu X, Yiu S-M, Lim BL. De novo assembly and characterization of *Camelina sativa* transcriptome by paired-end sequencing. *BMC Genomics* **14**, 146 (2013).

66. Grabherr MG*, et al.* Full-length transcriptome assembly from RNA-Seq data without a reference genome. *Nature Biotechnology* **29**, 644-652 (2011).

67. Lefort V, Longueville J-E, Gascuel O. SMS: Smart Model Selection in PhyML. *Molecular Biology and Evolution* **34**, 2422-2424 (2017).

68. Bordoli L, Kiefer F, Arnold K, Benkert P, Battey J, Schwede T. Protein structure homology modeling using SWISS-MODEL workspace. *Nature Protocols* **4**, 1-13 (2009).

69. Dundas J, Ouyang Z, Tseng J, Binkowski A, Turpaz Y, Liang J. CASTp: computed atlas of surface topography of proteins with structural and topographical mapping of functionally annotated residues. *Nucleic Acids Research* **34**, W116-W118 (2006).

70. Lopez-Obando M*, et al.* Structural modelling and transcriptional responses highlight a clade of PpKAI2-LIKE genes as candidate receptors for strigolactones in Physcomitrella patens. *Planta* **243**, 1441-1453 (2016).

ACKNOWLEDGEMENTS

This work was supported by funding from the Australian Research Council (DP130103646 to SMS and GRF; DP140104567 to SMS; FT150100162 to MTW, DP160102888 to GRF and

MTW). Y.K.S was recipient of a Research Training Program Scholarship from the Australian Government. We thank Dr Rowena Long for the original provision of *B. tournefortii* seeds, Dr Rohan Bythell-Douglas for advice on homology modelling, and Mr Yongjie Meng with assistance with RNA extractions. We are grateful to Dr Kevin Rozwadowski (Agriculture and Agri-Food Canada) for the provision of pSKI106.

CONTRIBUTIONS

Y.K.S., S.M.S., G.R.F. and M.T.W. conceived and designed the research; Y.K.S., A.S., J.Y., K.M. and M.T.W. performed the experiments; Y.K.S. and M.T.W. analysed the data; Y.K.S., S.M.S. and M.T.W. wrote the manuscript.

SUPPLEMENTARY INFORMATION

Supplementary Figure 1 Germination of *Brassica tournefortii* seed treated with karrikins

Supplementary Figure 2 Extended phylogeny of eu-KAI2 and D14 proteins in angiosperms

Supplementary Figure 3 Alignment of Brassica KAI2 sequences

Supplementary Figure 4 BtD14a is functionally homologous to AtD14

Supplementary Figure 5 Expression of BtKAI2 homologues in Arabidopsis and tobacco

Supplementary Figure 6 The *GFP-BtKAI2c* transgene is faithfully transcribed in Arabidopsis

Supplementary Figure 7 Germination profiles of transgenic Arabidopsis seeds expressing BtKAI2 homologues

Supplementary Figure 8 SDS-PAGE of SUMO-BtKAI2 fusion proteins used for DSF

Supplementary Figure 9 BtKAI2a and BtKAI2b do not respond to karrikins in DSF assays

Supplementary Figure 10 Stable transgenic expression of BtKAI2 valine–leucine exchange proteins in Arabidopsis

Supplementary Figure 11 Three experimental replicates of hypocotyl elongation assays with BtKAI2 Arabidopsis transgenics

Supplementary Table 1 List of sequences identified in this study

Supplementary Table 2 List of oligonucleotides

FIGURE LEGENDS

Figure 1. *Brassica tournefortii* is highly sensitive to KAR_1, the major karrikin analogue isolated from plant-derived smoke

a, Germination responses of *B. tournefortii* seed to KAR_1 and KAR_2. Data are cumulative germination after 11 days (mean ± SE; n = 3 biological replicates per treatment, ≥35 seeds per replicate). **b**, Levels of karrikin-responsive transcripts *BtDLK2* and *BtSTH7* in *B. tournefortii* seed. Seed were imbibed for 24 hours in the dark supplemented with KAR_1 and KAR_2. Transcripts were normalised to *BtCACS* reference transcripts. Data are means ± SE, n = 3 biological replicates, ≥50 seeds per replicate. **c**, **d**, Hypocotyl elongation responses of *B. tournefortii* seedlings treated with KAR_1 and KAR_2 and grown for four days under continuous red light. Data are means ± 95% CI of n = 18 to 24 seedlings. Scale bar: 10 mm. **e**, Levels of *BtDLK2* transcripts in *B. tournefortii* seedlings grown under the same conditions as for **d**. Data are means ± SE, n = 3 biological replicates, ≥20 seedlings per replicate. In all panels, asterisks denote significance levels (ANOVA) between indicated conditions: * P<0.05; ** P<0.01; *** P<0.001; **** P<0.0001.

Figure 2. Two differentially expressed *B. tournefortii KAI2* homologues are functional in *Arabidopsis*

a, Maximum likelihood phylogeny of KAI2 homologues in the Brassicaceae, based on nucleotide data. Node values represent bootstrap support from 100 replicates. A eu-KAI2 sequence from *Gossypium raimondii* (Malvaceae) serves as an outgroup. Tree shown is a subset of a larger phylogeny in Supplementary Fig. 2. **b**, Transcript levels of the three *BtKAI2* homologues in *B. tournefortii* seeds imbibed for 24 h (left) and four-day-old seedlings (right) treated with or without 1 µM KAR_1 for 24 h. **c**, **d**, Seedling and rosette phenotypes of two independent transgenic lines of Arabidopsis homozygous for *KAI2pro:GFP-BtKAI2* transgenes. Scale bars: 5 mm (**c**); 50 mm (**d**). **e**, Immunoblots of soluble proteins challenged with antibodies against KAI2 (upper panel), GFP (middle panel) or actin (lower panel). Non-specific bands are marked with asterisks. Protein was isolated from pools of approximately fifty 7-day-old seedlings.

Figure 3. Functional divergence between BtKAI2 homologues

a, Germination responses of primary dormant *Arabidopsis* seed homozygous for *KAI2pro:GFP-BtKAI2* transgenes in the *kai2-2* background. Germination values were determined 120 h after sowing. Extended germination curves are shown in Supplementary Fig. 7. Data are means ± SE, n = 3 independent seed batches, 75 seed per batch. **b**, Hypocotyl elongation responses of *KAI2pro:GFP-BtKAI2* seedlings treated with KAR_1 or KAR_2. Data are means ± SE of n = 3 biological replicates, 12–18 seedlings per replicate. **c**, Levels of *DLK2* transcripts in 8-day-old *KAI2pro:GFP-BtKAI2* seedlings treated with KAR_1 or KAR_2 for eight hours. Expression was normalised to *CACS* reference transcripts and scaled to the value for mock-treated seedlings within each genotype. Data are means ± SE of n = 3 biological replicates. Pairwise significant differences: * $P < 0.05$ ** $P < 0.01$ *** $P < 0.001$; ns, $P > 0.05$ (ANOVA).

Figure 4. Two residues account for ligand specificity between BtKAI2a and BtKAI2b

a, DSF curves of SUMO-BtKAI2a and SUMO-BtKAI2b fusion proteins treated with 0-50 µM $GR24^{ent\text{-}5DS}$, a KAI2-bioactive ligand. Each curve is the average of three sets of reactions, each comprising four technical replicates. Insets plot the minimum value of –(dF/dT) at the melting point of the protein as determined in the absence of ligand (means ± SE, n = 3). Significant differences from untreated control: * $P < 0.05$ ** $P < 0.01$ *** $P < 0.001$ (ANOVA). **b–e**, Homology models of BtKAI2a (b) and BtKAI2b (c), and solved structures of AtKAI2 (d, PDB: 3w06) and AtD14 (e, PDB: 4IH4). Coloured surfaces depict internal cavities; values indicate the volumes of the primary ligand-binding cavities, adjacent to the catalytic Ser-His-Asp residues. Also shown is a variable secondary pocket, to the left of the primary pocket in these images. **f**, DSF curves of SUMO-BtKAI2a$^{L98;L191}$ and SUMO-BtKAI2b $^{V98;V191}$ fusion proteins treated with 0-50 µM $GR24^{ent\text{-}5DS}$.

Figure 5. Substitutions between BtKAI2a and BtKAI2b at positions 98 and 191 reverse karrikin preference in transgenic Arabidopsis.

a, Hypocotyl elongation responses to karrikins in two independent transgenic lines homozygous for *GFP-BtKAI2a*$^{L98;L191}$ (3-5, 3-14) and two lines for *GFP-BtKAI2b*$^{V98;V191}$ (6-4, 6-13). Data shown are a summary of three experimental replicates performed on separate occasions, each comprising 20-40 seedlings per genotype/treatment combination. Data for each replicate are shown in Supplementary Figure 10. Error bars are SE, n=3 experimental replicates; each dot corresponds to the mean value derived from each replicate. Asterisks denote significant differences: * P<0.05, ** P<0.01, *** P<0.001, **** P<0.0001 (linear mixed model with experimental replicate as a random effect; specific pairwise comparisons using

Tukey's HSD correction). **b**, Levels of *DLK2* transcripts in the same transgenic lines treated with 1 µM KAR_1, 1 µM KAR_2, or 0.1% acetone and harvested 8 hours later. Expression was normalised to *CACS* reference transcripts. Data are means ± SE of n=3 pools of 50-100 seedlings treated in parallel. Asterisks denote significant differences as above (two-way ANOVA; specific pairwise comparisons using Tukey's HSD correction).

SUPPLEMENTARY FIGURE LEGENDS

Supplementary Figure 1. Germination of *Brassica tournefortii* seed treated with karrikins

a, Structures of KAR_1, KAR_2 and two enantiomers of GR24. **b**, Germination response of the "Merridin" batch of *B. tournefortii* seed treated with KAR_1 and KAR_2 after three days. **c-d**, Germination response of the "Perth" batch to KAR_1 (**c**) and KAR_2 (**d**). Data in Figure 1a are derived from the data shown in **c**. **e-f**, Uptake of KAR_1 and KAR_2 by imbibed seed, as determined by GC-MS. All error bars are mean ± SE of n = 3 batches of 75 seed (**b**-**d**) or 3 samples of 40 mg (**e**) or 20 mg (**f**) seed as described in Methods.

Supplementary Figure 2. Extended phylogeny of eu-KAI2 and D14 proteins in angiosperms

Maximum likelihood phylogeny of KAI2 and D14 homologues in the Brassicaceae and monocots, based on nucleotide data. Node values represent bootstrap support from 100 replicates. A KAI2 sequence from *Selaginella moellendorffii* (SmKAI2a; Waters et al. 2015) serves as an outgroup for the eu-KAI2 clade.

Supplementary Figure 3. Alignment of Brassica KAI2 sequences

Full length protein coding regions of *KAI2* homologues from four *Brassica* species (*Brassica tournefortii*, *B. rapa*, *B. nigra* and *B. oleracea*) were translated from database nucleic acid sequences and aligned to *Arabidopsis thaliana* KAI2 using MAFFT (Katoh et al, 2002) implemented in Geneious R10 software (Biomatters Ltd). Amino acid residues are coloured according to polarity: yellow, non-polar (G, A, V, L, I, F, W, M, P); green, polar & uncharged (S, T, C, Y, N, Q); red, polar & acidic (D, E); blue, polar & basic (K, R, H). Residues that are unique to BtKAI2c but otherwise invariant are highlighted with asterisks (*); residues 98 and 191 are highlighted with red boxes.

Supplementary Figure 4. BtD14a is functionally homologous to AtD14

Three independent transgenic lines of Arabidopsis *Atd14-1* were analysed for functional complementation of the mutant phenotype by an *AtD14pro:BtD14a* transgene. **a**, Rosette and leaf morphology at 31 days post-germination. **b**, Plant height and number of primary rosette branches at 45 days post-germination. **c**, Quantification of height and branching parameters, *n* = 10 plants per genotype. Scale bars: 50 mm.

Supplementary Figure 5. Expression of BtKAI2 homologues in Arabidopsis and tobacco

a, Quantitative RT-PCR analysis of *GFP* and *DLK2* transcripts, normalised to *CACS* reference transcripts. Data are derived from a single biological sample with four technical PCR replicates. RNA was isolated from approximately 50 seven-day-old seedlings per genotype, and are the same samples as those shown in the immunoblots in Figure 2d. **b**, Alignment of the protein regions corresponding to the peptide epitope TTNPDYFDFDRYSN of AtKAI2, against which the anti-KAI2 peptide was raised. BtKAI2b, with a more divergent epitope, is relatively poorly detected by the anti-KAI2 antibody (see Figure 2d). **c**, Transient expression of BtKAI2a, BtKAI2b and BtKAI2c proteins in tobacco. Plasmids encoding N-terminal, *c*-myc-tagged proteins were transferred to *Agrobacterium*, and the resulting strains used to infiltrate tobacco leaves. After 96 h, samples were harvested in triplicate (two to three leaves per sample). Mock-treated leaves were transformed with a plasmid encoding a non-tagged protein. Sixty micrograms of total protein were separated by SDS-PAGE, blotted and challenged with anti-*c*-myc antibody (Genscript A00704). Band intensity was measured using ImageJ, and expression was normalised to intensity of the Rubisco large subunit (RbcL) band on the "stain-free" gel imaged under UV light. Error bars indicate SE, *n* = 3 replicates.

Supplementary Figure 6. The GFP-BtKAI2c transgene is faithfully transcribed in Arabidopsis

a, Structure of the *AtKAI2pro:mGFP6-BtKAI2c* transgene. Primers used for RT-PCR are shown with arrows. The promoter and 5′UTR are derived from *At4g37470* (*AtKAI2*). attB1, Gateway recombination site that links *mGFP6* and *BtKAI2c* regions; *nos ter*, nopaline synthase terminator. Not drawn to scale. **b**, RT-PCR analysis of *GFP-BtKAI2c* transcripts after 35 cycles of amplification. Primers MW406 + BK010 target the transgene, while a second primer pair (MW275 + MW278) serves as a control and spans five introns of *At1g03055*. *kai2-2* serves as a non-transgenic control genotype. Templates: R, total RNA; D, genomic DNA; W, water only. RT, reverse transcriptase (Supercript III). DNA size standards (in base pairs) are indicated on the left, with anticipated PCR product sizes shown on the right and defined in the table. **c**, The RT-

PCR product generated with proof-reading polymerase (Q5, New Engalnd Biolabs) and primers MW406 and BK010 was cloned into pCR4-TOPO (Life Technologies). Five dideoxy sequence traces were aligned against the *GFP-BtKAI2c* transgene reference. No disagreements with the reference sequence were observed. Red bars indicate trimmed regions of sequence traces to remove low quality data.

Supplementary Figure 7. Germination profiles of transgenic Arabidopsis seeds expressing BtKAI2 homologues

Freshly harvested seed (three batches per genotype, each batch harvested from four plants) were removed from freezer storage, surface-sterilised and sown on 1% Phytagel supplemented with 0.1% acetone (mock), 1 µM KAR_1 or 1 µM KAR_2. Seed were incubated under constant light at 25 °C. Seed were examined for germination (radicle protrusion) 72 h after sowing and every 24 h thereafter. Data are means ± SE of three independent seed batches and 75 seed per batch. For each transgene, two independent, homozygous transgenic lines were analysed. Data presented in Figure 3 of the main manuscript are derived from these data.

Supplementary Figure 8. SDS-PAGE of SUMO-BtKAI2 fusion proteins used for DSF

To assess purity after affinity chromatography, five micrograms of each purified protein was electrophoresed on a 12% acrylamide gel containing 2,2,2-trichloroethanol and visualised under UV light. Protein size standards at 75 and 25 kDa (Bio-Rad Precision Plus Dual Colour) fluoresce strongly under UV light.

Supplementary Figure 9. BtKAI2a and BtKAI2b do not respond to karrikins in DSF assays

Differential scanning fluorimetry curves of BtKAI2a and BtKAI2b in presence of 0–200 µM KAR_1 or KAR_2 (**a**) or the two enantiomers of GR24 (**b**). Data are means of eight technical replicates at each concentration of ligand.

Supplementary Figure 10. Stable transgenic expression of BtKAI2 valine–leucine exchange proteins in Arabidopsis

a, Immunoblots of total soluble protein extracted from 7-day-old seedlings of independent transgenic lines segregating in a 3:1 ratio for hygromycin resistance. Transgene expression in six lines expressing *GFP-BtKAI2a*$^{L98;L191}$ (upper panels) and five expressing *GFP-BtKAI2b*$^{V98;V191}$ (lower panels) were compared to a representative unmodified control (*GFP-BtKAI2a* 1F and *GFP-BtKAI2b* 9A respectively). Based on expression level two lines of each construct (3-5 and 3-14; 6-4 and 6-13) were selected and brought to homozygosity for further experiments. Protein blots were challenged with anti-GFP antibody. Equal gel loading was assessed by

865 imaging total protein prior to blotting; the RbcL band is shown. **b**, Rosette phenotypes of
866 homozygous individuals expressing native and modified *GFP-BtKAI2* transgenes. Plants were
867 25 days old and grown under long day conditions as described in Methods. Scale bar: 50 mm.

868 **Supplementary Figure 11. Three experimental replicates of hypocotyl elongation assays**
869 **with BtKAI2 Arabidopsis transgenics**
870 Each panel depicts data from an independent experiment performed on a separate date, which
871 are shown in summarised format in Figure 5. Data are means ± SE, n=24 to 40 seedlings. Each
872 dot corresponds to an individual seedling.

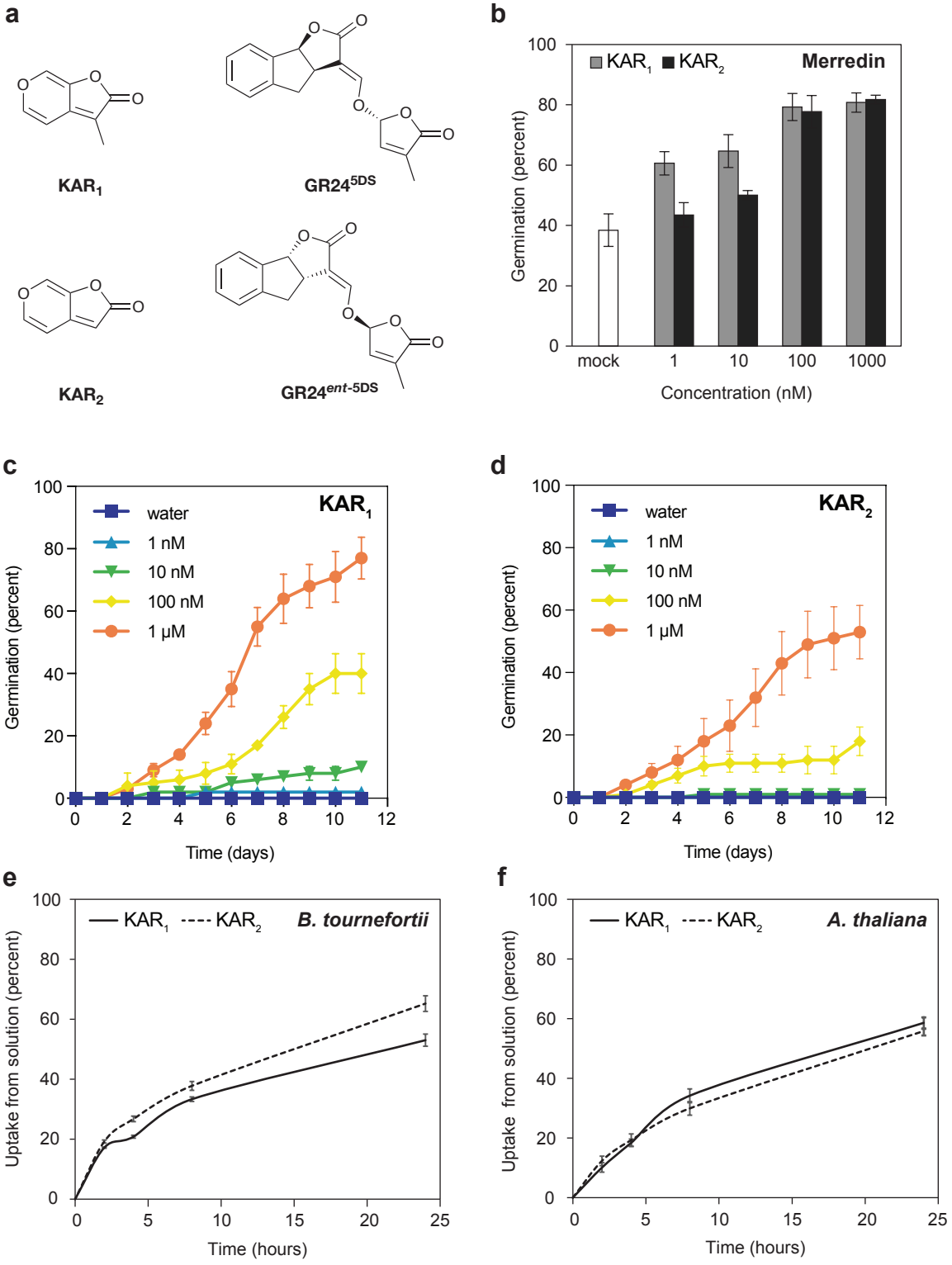

Supplementary Figure 1. Germination of *Brassica tournefortii* seed treated with karrikins
a, Structures of KAR_1, KAR_2 and two enantiomers of GR24. **b,** Germination response of the "Merridin" batch of *B. tournefortii* seed treated with KAR_1 and KAR_2 after three days. **c-d,** Germination response of the "Perth" batch to KAR_1 (**c**) and KAR_2 (**d**). Data in Figure 1a are derived from the data shown in **c.** **e-f**, Rates of KAR_1 and KAR_2 uptake by imbibed seed, as determined by GC-MS. All error bars are mean ± SE of n = 3 batches of 75 seed (b-d) or 3 samples of 40 mg (e) or 20 mg (f) seed as described in Methods.

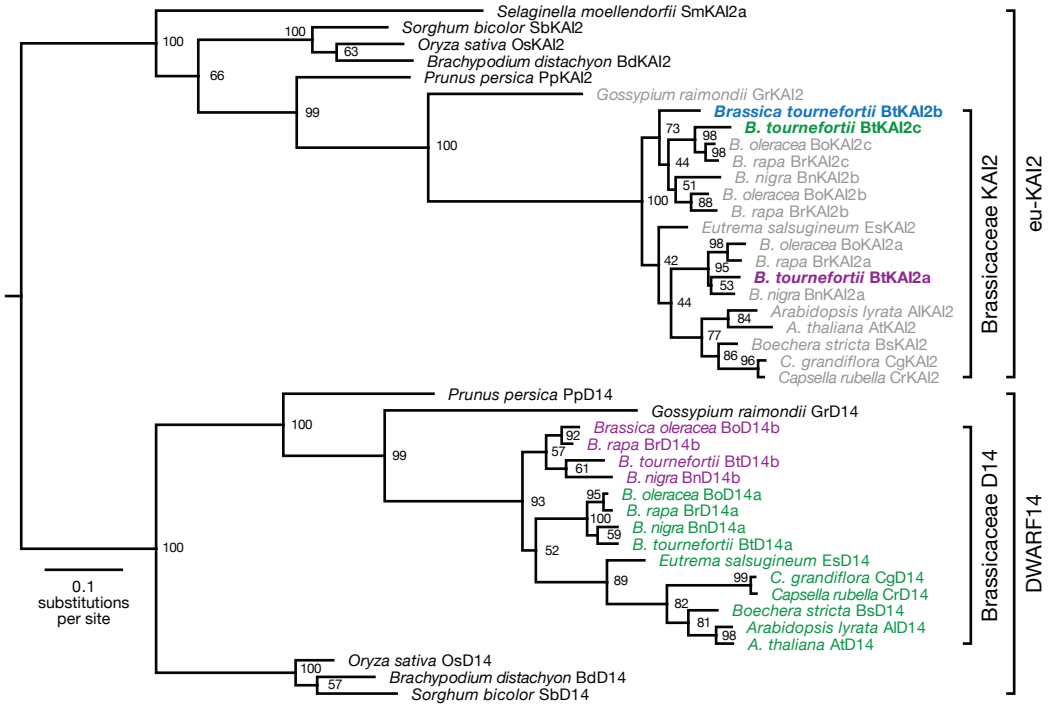

Supplementary Figure 2. Extended phylogeny of eu-KAI2 and D14 proteins in angiosperms
Maximum likelihood phylogeny of KAI2 and D14 homologues in the Brassicaceae and monocots, based on nucleotide data. Node values represent bootstrap support from 100 replicates. A KAI2 sequence from *Selaginella moellendorffii* (SmKAI2a; Waters et al. 2015) serves as an outgroup for the eu-KAI2 clade.

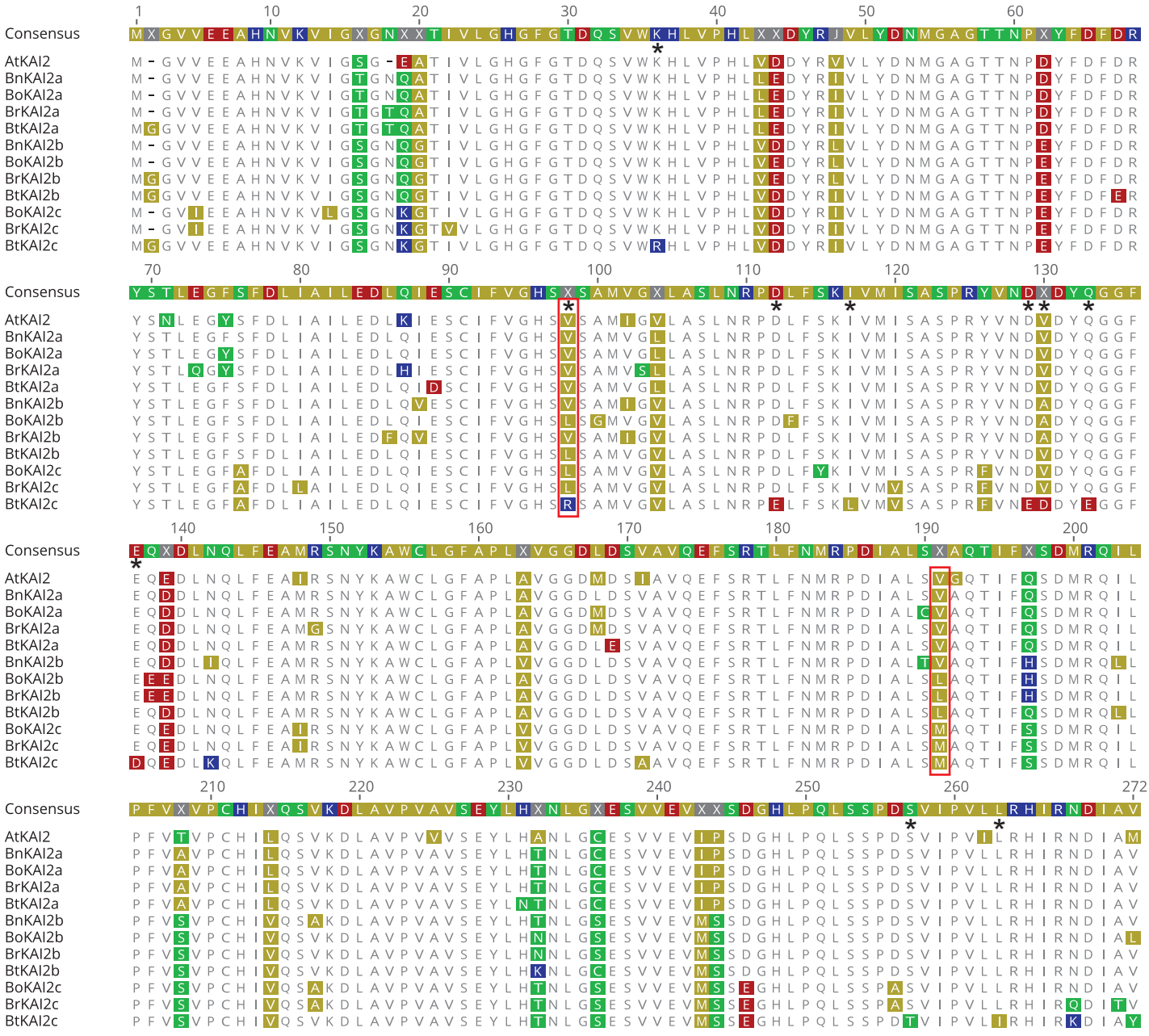

Supplementary Figure 3. Alignment of *Brassica* KAI2 sequences

Full length protein coding regions of KAI2 homologues from four *Brassica* species (*Brassica tournefortii*, *B. rapa*, *B. nigra* and *B. oleracea*) were translated from database nucleic acid sequences and aligned to Arabidopsis KAI2 using MAFFT (Katoh et al, 2002) implemented in Geneious R10 software (Biomatters Ltd). Amino acid residues are coloured according to polarity: yellow, non-polar (G, A, V, L, I, F, W, M, P); green, polar & uncharged (S, T, C, Y, N, Q); red, polar & acidic (D, E); blue, polar & basic (K, R, H). Residues that are unique to BtKAI2c but otherwise invariant are highlighted with asterisks (*); residues 98 and 191 are highlighted with red boxes.

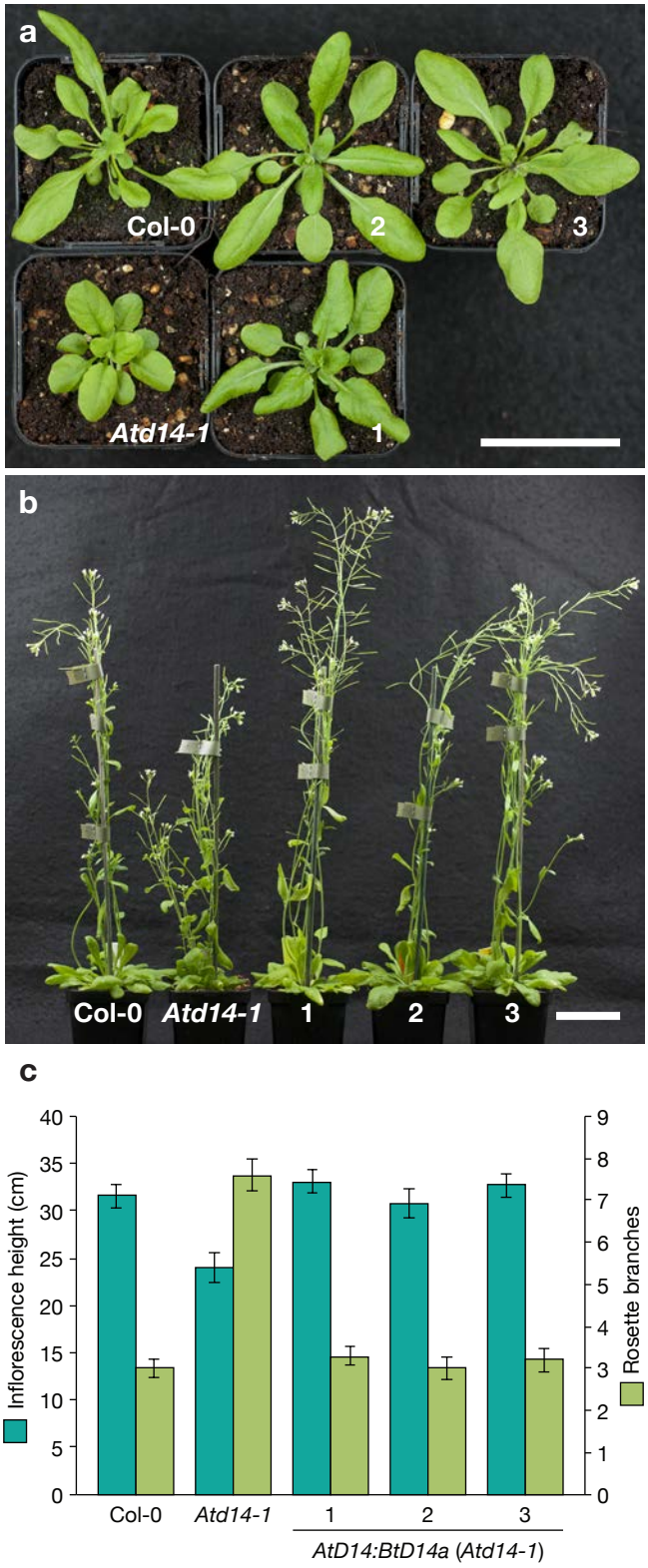

Supplementary Figure 4. BtD14a is functionally homologous to AtD14
Three independent transgenic lines of Arabidopsis *Atd14-1* were analysed for functional complementation of the mutant phenotype by an *AtD14pro:BtD14a* transgene. **a**, Rosette and leaf morphology at 31 days post-germination. **b**, Plant height and number of primary rosette branches at 45 days post-germination. **c**, Quantification of height and branching parameters, means ± SE, *n* = 10 plants per genotype. Scale bars: 50 mm.

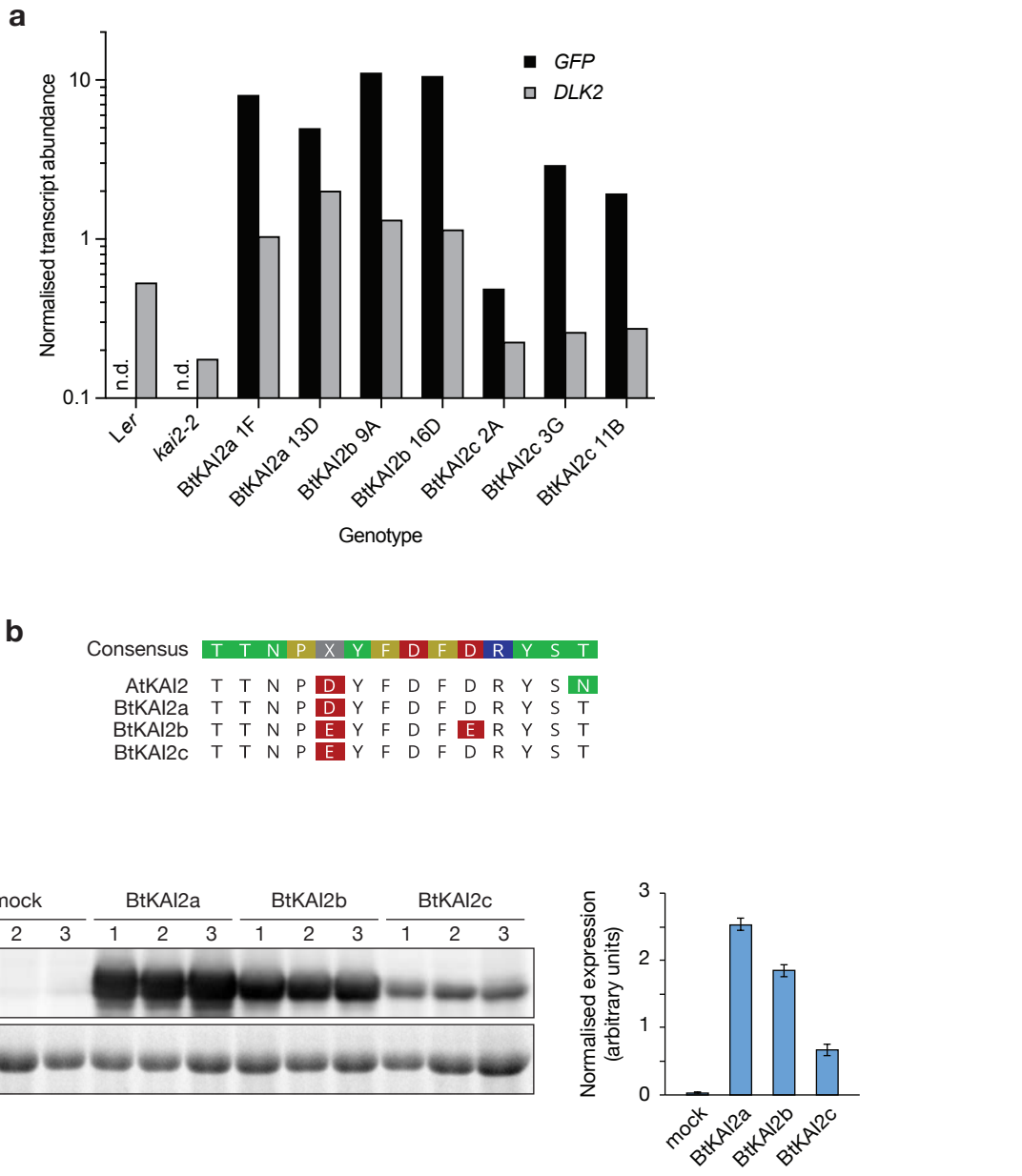

Supplementary Figure 5. Expression of BtKAI2 homologues in Arabidopsis and tobacco
a, Quantitative RT-PCR analysis of *GFP* and *DLK2* transcripts, normalised to *CACS* reference transcripts. Data are derived from a single biological sample with four technical PCR replicates. RNA was isolated from approximately 50 seven-day-old seedlings per genotype, and are the same samples as those shown in the immunoblots in Figure 2. **b**, Alignment of the protein regions corresponding to the peptide epitope TTNPDYFDFDRYSN of AtKAI2, against which the anti-KAI2 peptide was raised. BtKAI2b, with a more divergent epitope, is relatively poorly detected by the anti-KAI2 antibody (see Figure 2). **c**, Transient expression of BtKAI2a, BtKAI2b and BtKAI2c proteins in tobacco. Plasmids encoding N-terminal, c-myc-tagged proteins were transferred to Agrobacterium, and the resulting strains used to infiltrate tobacco leaves. After 96 h, samples were harvested in triplicate (two to three leaves per sample). Mock-treated leaves were transformed with a plasmid encoding a non-tagged protein. Sixty micrograms of total protein were separated by SDS-PAGE, blotted and challenged with anti-c-myc antibody (Genscript A00704). Band intensity was measured using ImageJ, and expression was normalised to intensity of the Rubisco large subunit (RbcL) band on the “stain-free” gel imaged under UV light. Error bars indicate SE, *n* = 3 replicates.

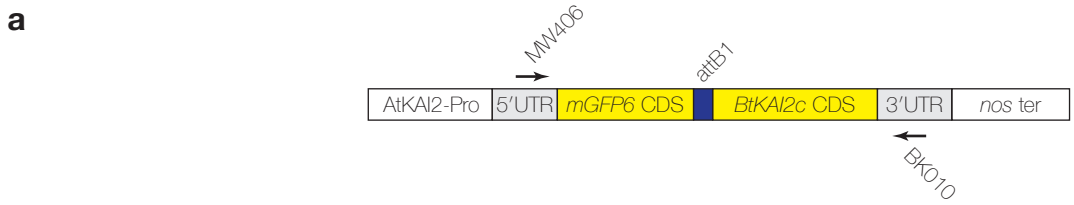

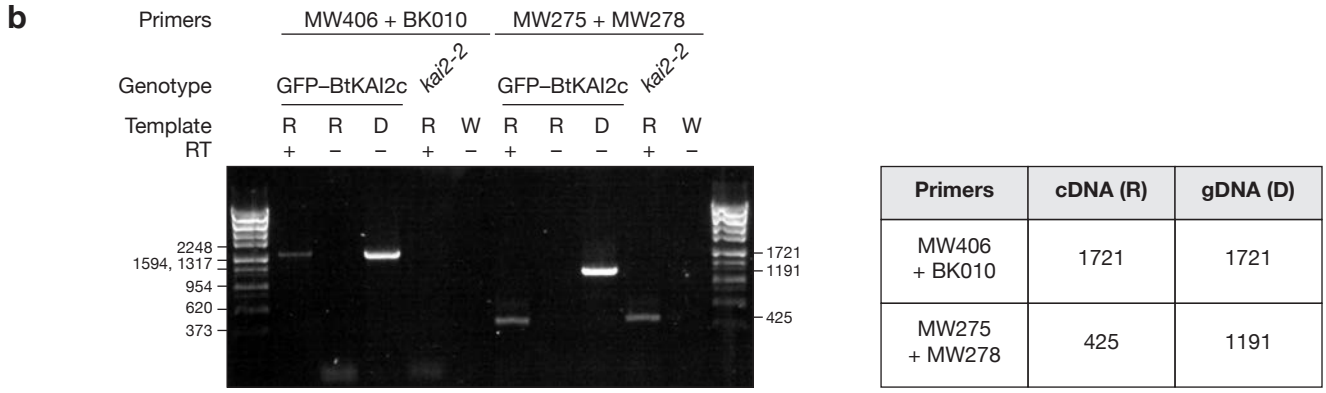

Primers	cDNA (R)	gDNA (D)
MW406 + BK010	1721	1721
MW275 + MW278	425	1191

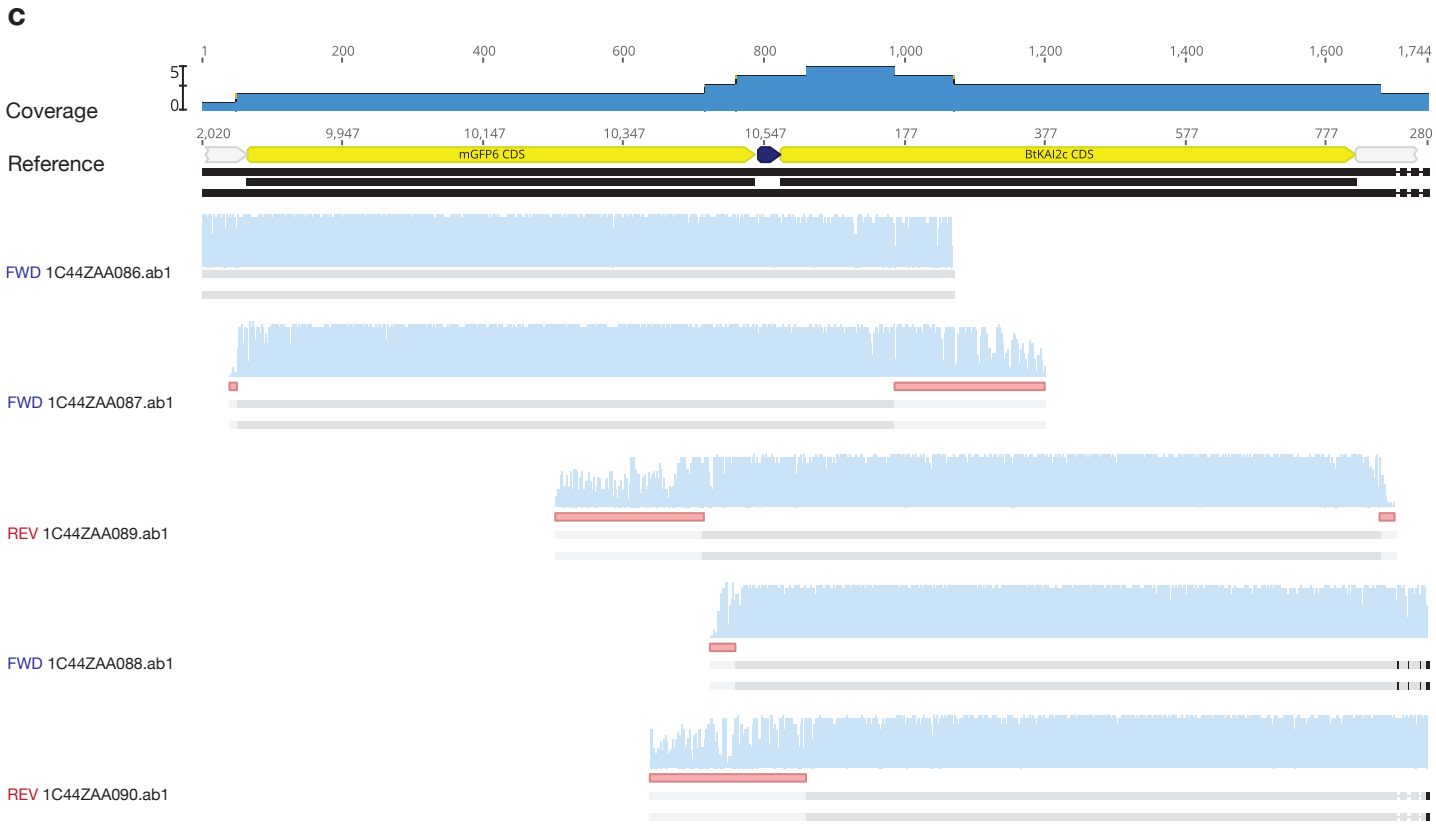

Supplementary Figure 6. The *GFP-BtKAI2c* transgene is faithfully transcribed in Arabidopsis

a, Structure of the *AtKAI2pro:mGFP6-BtKAI2c* transgene. Primers used for RT-PCR are shown with arrows. The promoter and 5′UTR are derived from *At4g37470* (*AtKAI2*). attB1, Gateway recombination site that links mGFP6 and BtKAI2c regions; *nos* ter, nopaline synthase terminator. Not drawn to scale.

b, RT-PCR analysis of *GFP-BtKAI2c* transcripts after 35 cycles of amplification. Primers MW406 + BK010 target the transgene, while a second primer pair (MW275 + MW278) serves as a control and spans five introns of *At1g03055*. *kai2-2* serves as a non-transgenic control genotype. Templates: R, total RNA; D, genomic DNA; W, water only. RT, reverse transcriptase (Supercript III). DNA size standards (in base pairs) are indicated on the left, with anticipated PCR product sizes shown on the right and defined in the table.

c, The RT-PCR product generated with proof-reading polymerase (Q5, New Engalnd Biolabs) and primers MW406 and BK010 was cloned into pCR4-TOPO (Life Technologies). Five dideoxy sequence traces were aligned against the *GFP-BtKAI2c* transgene reference. No disagreements with the reference sequence were observed. Red bars indicate trimmed regions of sequence traces to remove low quality data.

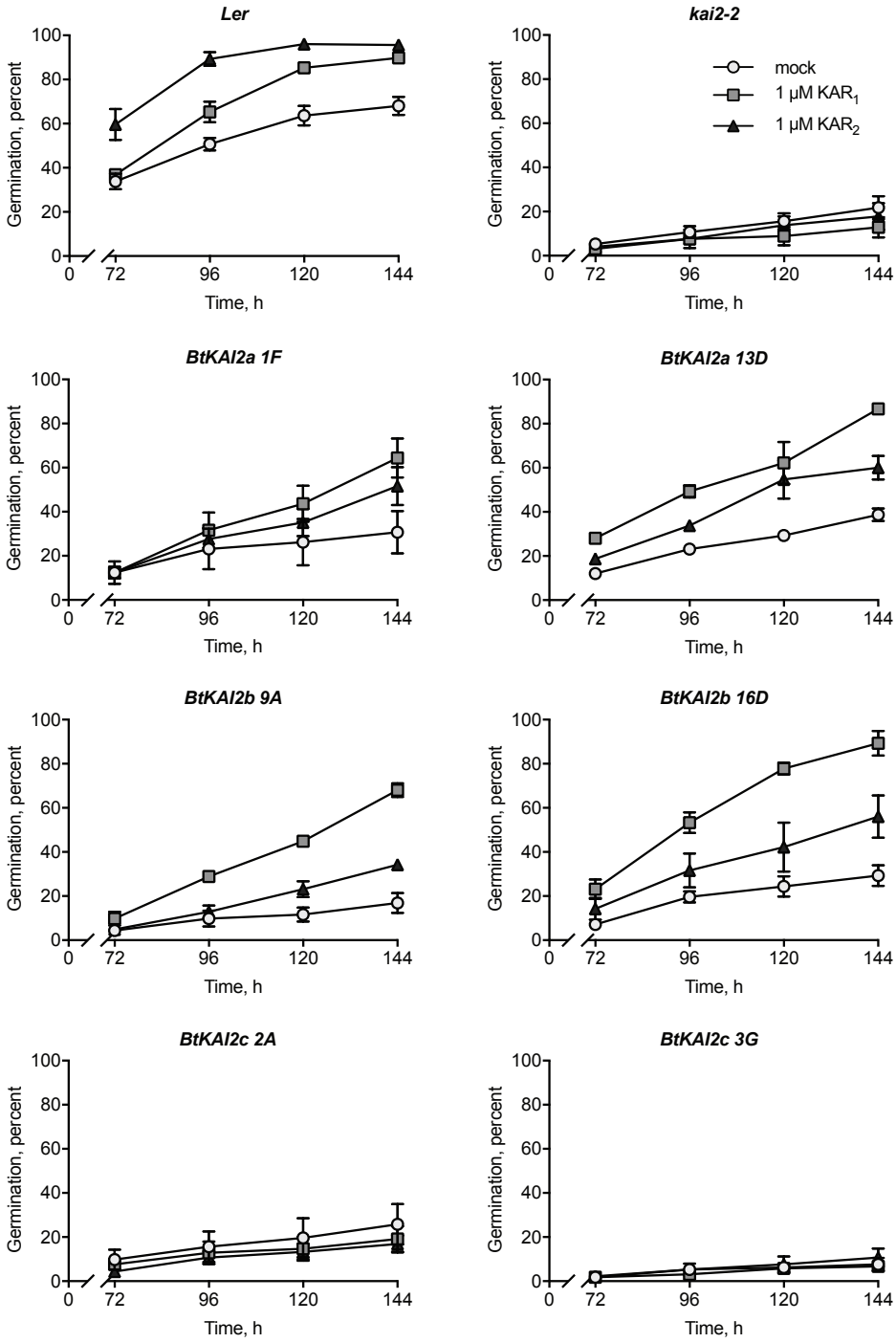

Supplementary Figure 7. Germination profiles of transgenic Arabidopsis seeds expressing BtKAI2 homologues
Freshly harvested seed (three batches per genotype, each batch harvested from four plants) were removed from freezer storage, surface-sterilised and sown on 1% Phytagel supplemented with 0.1% acetone (mock), 1 µM KAR_1 or 1 µM KAR_2. Seed were incubated under constant light at 25 °C. Seed were examined for germination (radicle protrusion) 72 h after sowing and every 24 h thereafter. Data are means ± SE of three independent seed batches and 75 seed per batch. For each transgene, two independent, homozygous transgenic lines were analysed. Data presented in Figure 3 of the main manuscript are derived from these data.

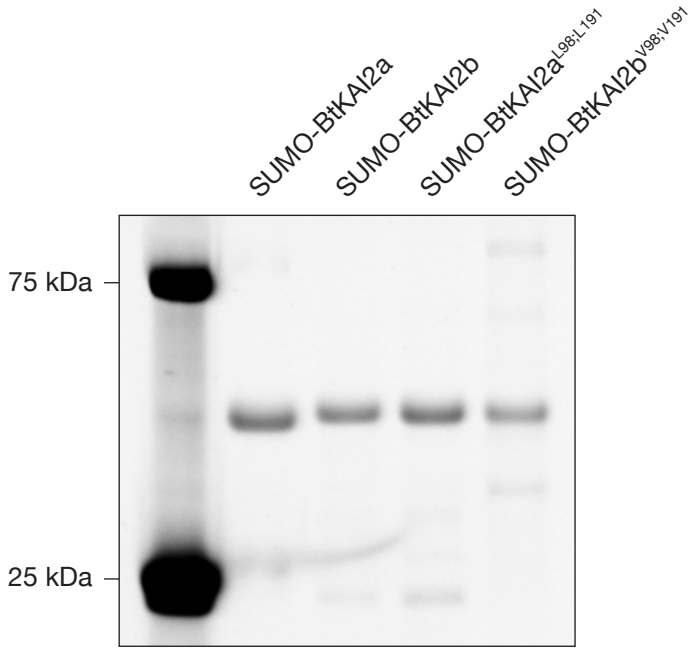

Supplementary Figure 8. SDS-PAGE of SUMO-BtKAI2 fusion proteins used for DSF.
To assess purity after affinity chromatography, five micrograms of each purified protein was electrophoresed on a 12% acrylamide gel containing 2,2,2-trichloroethanol and visualised under UV light. Protein size standards at 75 and 25 kDa (Bio-Rad Precision Plus Dual Colour) fluoresce strongly under UV light.

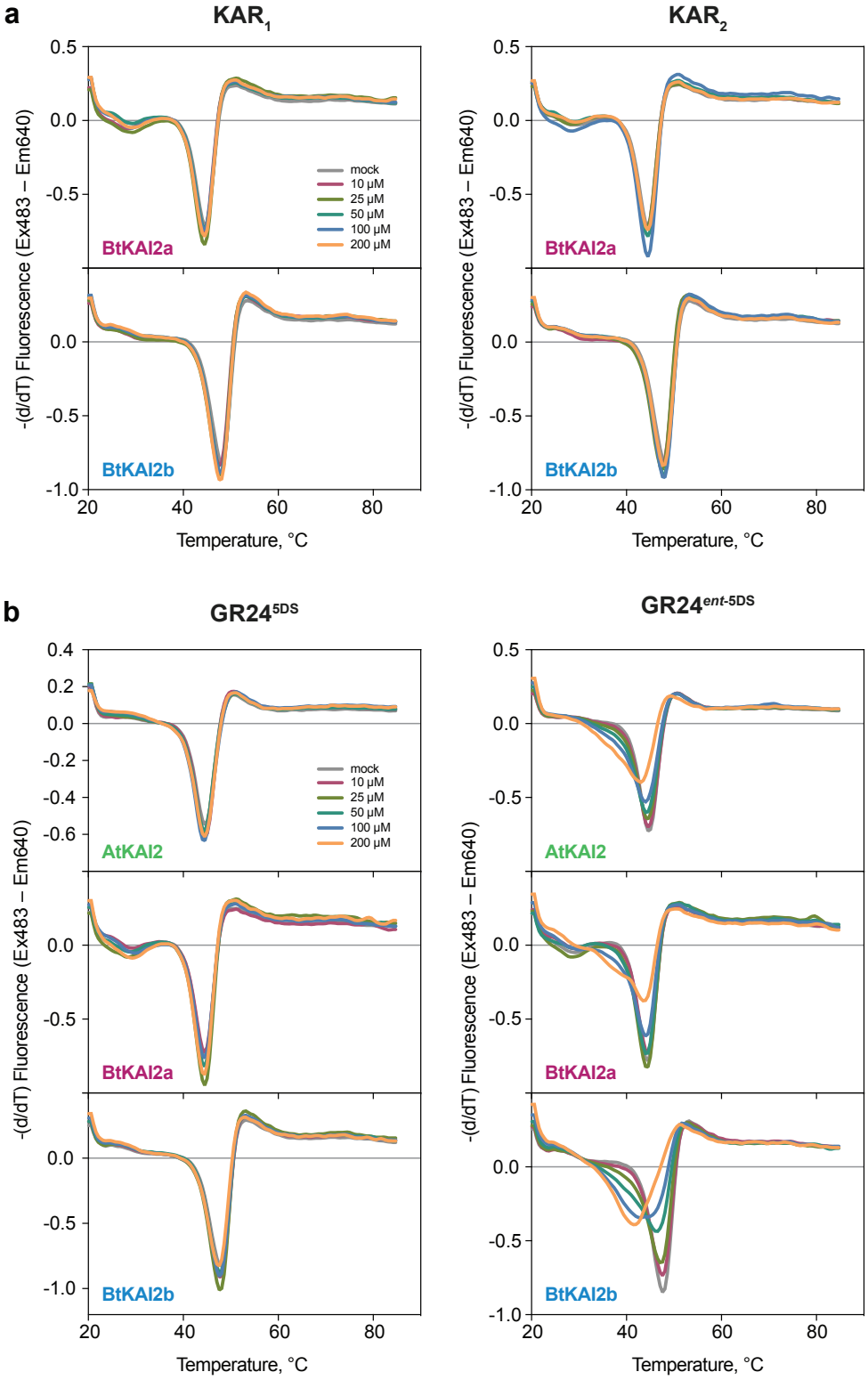

Supplementary Figure 9. BtKAI2a and BtKAI2b do not respond to karrikins in DSF assays
Differential scanning fluorimetry curves of SUMO-BtKAI2a and SUMO-BtKAI2b in presence of 0–200 µM KAR_1 or KAR_2 (**a**) or the two enantiomers of GR24 (**b**). Data are means of eight technical replicates at each concentration of ligand.

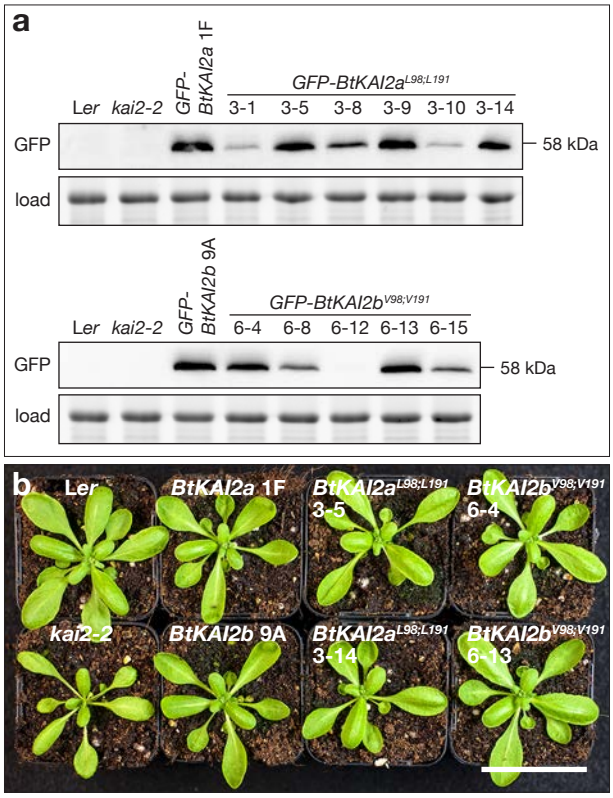

Supplementary Figure 10. Stable transgenic expression of BtKAI2 valine–leucine exchange proteins in Arabidopsis

a, Immunoblots of total soluble protein extracted from 7-day-old seedlings of independent transgenic lines segregating in a 3:1 ratio for hygromycin resistance. Transgene expression in six lines expressing GFP-BtKAI2a$^{L98;L191}$ (upper panels) and five expressing GFP-BtKAI2b$^{V98;V191}$ (lower panels) were compared to a representative unmodified control (GFP-BtKAI2a 1F and GFP-BtKAI2b 9A respectively). Based on expression level two lines of each construct (3-5 and 3-14; 6-4 and 6-13) were selected and brought to homozygosity for further experiments. Protein blots were challenged with anti-GFP antibody. Equal gel loading was assessed by imaging total protein prior to blotting; the RbcL band is shown. **b**, Rosette phenotypes of homozygous individuals expressing native and modified *GFP-BtKAI2* transgenes. Plants were 25 days old and grown under long day conditions as described in Methods. Scale bar: 50 mm.

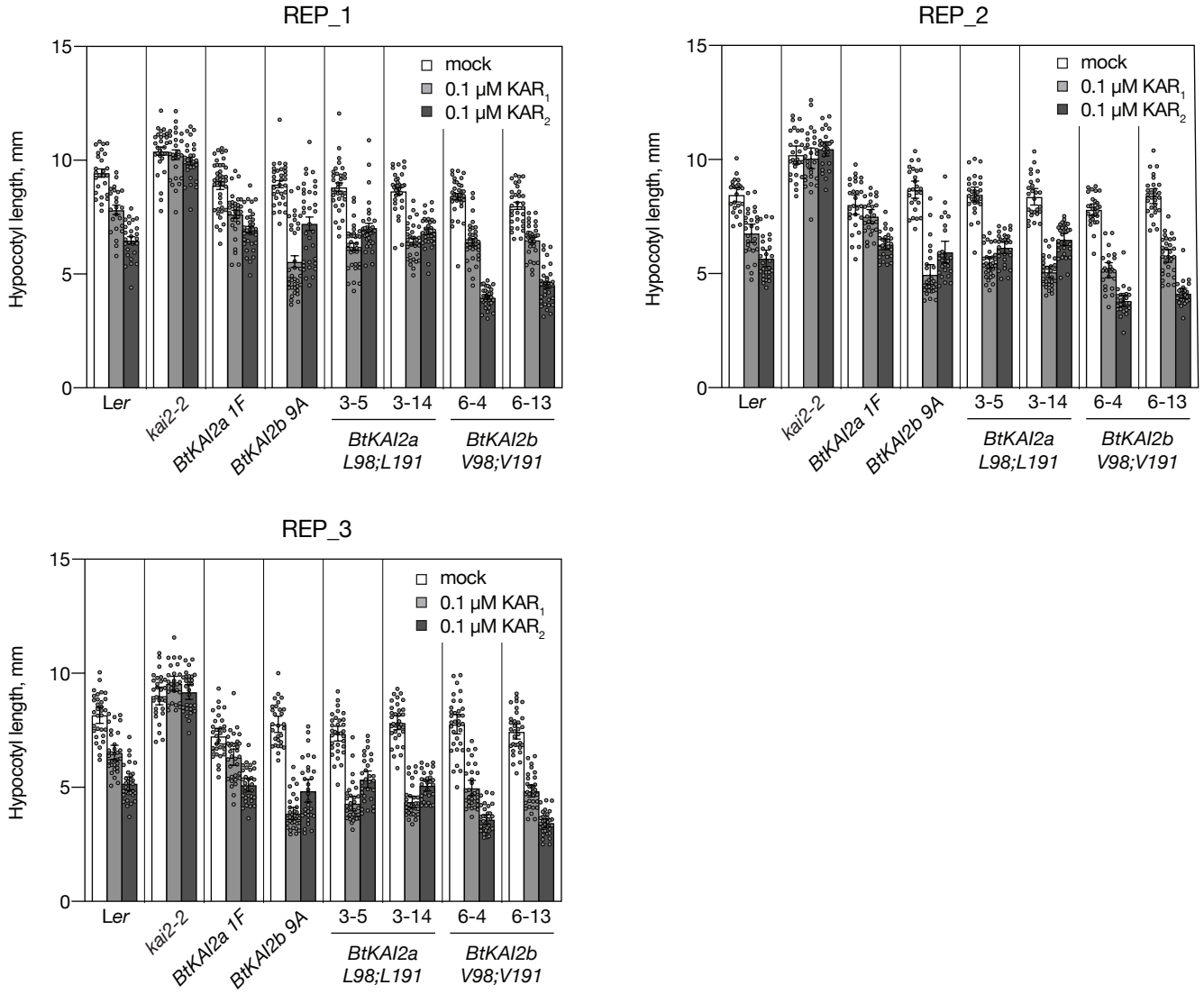

Supplemental Figure 11. Three experimental replicates of hypocotyl elongation assays with BtKAI2 Arabidopsis-transgenics

Each panel depicts data from an independent experiment performed on a separate date, which are shown in summarised format in Figure 5. Data are means ± SE, n=24 to 40 seedlings. Each dot corresponds to an individual seedling.

Supplementary Table 1. List of sequences identified in this study

KAI2

Species	Gene name	Sequence ID	Source	Reference
Arabidopsis lyrata	*AlKAI2*	AL7G13320.t1	Phytozome	This work
Arabidopsis thaliana	*AtKAI2*	At3g37470	TAIR	Waters et al (2012)
Brassica tournefortii (saharan mustard)	*BtKAI2a*	MG783328	GenBank/NCBI	This work
Brassica tournefortii (saharan mustard)	*BtKAI2b*	MG783329	GenBank/NCBI	This work
Brassica tournefortii (saharan mustard)	*BtKAI2c*	MG783330	GenBank/NCBI	This work
Brassica rapa (field mustard, AA genome)	*BrKAI2a*	XM_009111126.2	GenBank/NCBI	This work
Brassica rapa (field mustard, AA genome)	*BrKAI2b*	XM_009140247	GenBank/NCBI	This work
Brassica rapa (field mustard, AA genome)	*BrKAI2c*	XM_009144693	GenBank/NCBI	This work
Brassica nigra (black mustard, BB genome)	*BnKAI2a*	LFLV01000699.1	GenBank/NCBI	This work
Brassica nigra (black mustard, BB genome)	*BnKAI2b*	LFLV01001772.1	GenBank/NCBI	This work
Brassica oleracea (cabbage, CC genome)	*BoKAI2a*	XM_013766720.1	Phytozome	This work
Brassica oleracea (cabbage, CC genome)	*BoKAI2b*	XM_013738288.1	Phytozome	This work
Brassica oleracea (cabbage, CC genome)	*BoKAI2c*	XM_013778816.1	Phytozome	This work
Boechera stricta	*BsKAI2*	Bostr.30440s0001.1	Phytozome	This work
Capsella rubella	*CrKAI2*	Carubv10005485m	Phytozome	This work
Capsella grandiflora	*CgKAI2*	Cagra.1232s0005.1	Phytozome	This work
Eutrema salsugineum	*EsKAI2*	Thalv10025969m	Phytozome	Bythell-Douglas et al (2017)
Gossypium raymondii	*GrKAI2*	Gorai.003G028500.1	Phytozome	Bythell-Douglas et al (2017)
Prunus persica	*PpKAI2*	Ppa009957m	Phytozome	Bythell-Douglas et al (2017)
Brachypodium distachyon	*BdKAI2*	Bradi1g15880.1	Phytozome	Bythell-Douglas et al (2017)
Oryza sativa	*OsKAI2*	Os03g32270.1	Phytozome	Bythell-Douglas et al (2017)
Sorghum bicolor	*SbKAI2*	Sorbic.001G330000.1	Phytozome	Bythell-Douglas et al (2017)
Selaginella moellendorffii	*SmKAI2a*	Selmo_441991	Phytozome	Waters et al (2015)

D14

Species	Gene name	Sequence ID	Source	Reference
Arabidopsis lyrata	*AlD14*	AL3G13900.t1	Phytozome	This work
Arabidopsis thaliana	*AtD14*	AT3G03990.1	TAIR	Waters et al (2012)
Brassica oleracea (cabbage, CC genome)	*BoD14a*	LOC106343216	Phytozome	This work
Brassica oleracea (cabbage, CC genome)	*BoD14b*	LOC106343689	Phytozome	This work
Brassica nigra (black mustard, BB genome)	*BnD14a*	LFLV01002090	GenBank/NCBI	This work
Brassica nigra (black mustard, BB genome)	*BnD14b*	LFLV01000699	GenBank/NCBI	This work
Brassica rapa (field mustard, AA genome)	*BrD14a*	Brara.A03790	Phytozome	This work
Brassica rapa (field mustard, AA genome)	*BrD14b*	Brara.E03476	Phytozome	This work
B. tournefortii (saharan mustard)	*BtD14a*	MG783331	Phytozome	This work
B. tournefortii (saharan mustard)	*BtD14b*	MG783332	Phytozome	This work
Boechera stricta	*BsD14*	Bostr.2570s0310	Phytozome	This work
Capsella grandiflora	*CgD14*	Cagra.15970s0001	Phytozome	This work
Capsella rubella	*CrD14*	Carubv10014401m	Phytozome	This work
Eutrema salsugineum	*EsD14*	Thhalv10021292m	Phytozome	Bythell-Douglas et al (2017)
Gossypium raymondii	*GrD14*	Gorai.010G025600.1	Phytozome	Bythell-Douglas et al (2017)
Prunus persica	*PpD14*	ppa010005m	Phytozome	Bythell-Douglas et al (2017)
Brachypodium distachyon	*BdD14*	Bradi1g70930.3	Phytozome	Bythell-Douglas et al (2017)
Oryza sativa	*OsD14*	Os03g10620.1	Phytozome	Bythell-Douglas et al (2017)
Sorghum bicolor	*SbD14*	Sobic.001G465100.1	Phytozome	Bythell-Douglas et al (2017)

DLK2

Species	Gene name	Sequence ID	Source	Reference
B. tournefortii (saharan mustard)	*BtDLK2*	MG783333	GenBank/NCBI	This work

Supplementary Table 2. Oligonucleotides used in this study

Oligonucleotide	Sequence	Notes
Cloning		
BtD14a_F	AAAAAAGCAGGCTTCCATTATGAGTCAACACAACAT	BtD14a
BtD14a_R	CAAGAAAGCTGGGTTTTAAAGTCACCGAGGAAG	BtD14a
BtKAI2_universal_F	GGGGACAAGTTTGTACAAAAAAGCAGGCTTCATGGGAGGTGTGGTAGAGGA	All BtKAI2
RACE_R	GGGGACCACTTTGTACAAGAAAGCTGGGTCATTCTCAATAGACAATAGAC	BtKAI2a
Contig1_R	GGGGACCACTTTGTACAAGAAAGCTGGGTCCGAAACGACCCACTCACTTACC	BtKAI2b
Contig5_R	GGGGACCACTTTGTACAAGAAAGCTGGGTCCGAAGCAGAACCAAGCTAA	BtKAI2c
BtKAI2-SUMO-Gib_F	TGAGGCTCACCGCGAACAGATTGGAGGTATGGGAGGTGTGGTAGAGGAAG	pSUMO-BtKAI2a / BtKAI2b
BtKAI2a-SUMO-Gib_R	CGGATCTCAGTGGTGGTGGTGGTGGTGCTCAGACAGCGATGTCATTACGA	pSUMO-BtKAI2a
BtKAI2b-SUMO-Gib_R	CGGATCTCAGTGGTGGTGGTGGTGGTGCTCATACAGCAATGTCGTTGCGG	pSUMO-BtKAI2b
BtKAI2b_L98V_F1	ATCTTTGTTGGTCACTCTGTCTCCGCCATG	For BtKAI2b(a) mutagenesis
BtKAI2b_L191V_R1	TTTGGAAAATGGTCTGAGCCACGGAGAGTG	For BtKAI2b(a) mutagenesis
BtKAI2b_L191V_F2	TCTCCGTGGCTCAGACCATTTTCCAAAGC	For BtKAI2b(a) mutagenesis
BtKAI2b_L98V_R2	CATGGCGGAGACAGAGTGACCAACAAAG	For BtKAI2b(a) mutagenesis
BtKAI2a_V98L_F1	ATCTTTGTTGGTCACTCTCTCTCCGCCATG	For BtKAI2a(b) mutagenesis
BtKAI2a_V191L_R1	TTTGGAAAATGGTCTGAGCCAGGGAGAGAG	For BtKAI2a(b) mutagenesis
BtKAI2a_V191L_F2	TCTCCCTGGCTCAGACCATTTTCCAAAG	For BtKAI2a(b) mutagenesis
BtKAI2a_V98L_R2	CATGGCGGAGAGAGAGTGACCAACAAAG	For BtKAI2a(b) mutagenesis
MW406	CACGAACTGACTAAGAGAGG	For cloning GFP-BtKAI2c cDNA
BK010	GAAACGATATACTCAGTACTTACCAC	For cloning GFP-BtKAI2c cDNA
Quantitative PCR		
BtSTH7_qF	CATCTCCGGTTCTCTCTCACTTCT	Designed against At4g39070
BtSTH7_qR	CATTCTCTGCATAGTATTGCTCTGTC	Designed against At4g39070
BtDLK2_qF	GCTGCTTCTCCCAGGTATATAA	BtDLK2
BtDLK2_qR	GAAAGCAACCGCCCAAGCC	BtDLK2
AtDLK2_qF	GCTGCTTCTCCAAGGTATATAA	Designed against At3g24420
AtDLK2_qR	GAAATCAACCGCCCAAGCT	Designed against At3g24420
BtKAI2_universal_qF	GGTCATCTTCCTCAGCTTAG	All BtKAI2
BtKAI2_a_qR1	CCATTAATTTAATTTAAAATCACTTCCC	BtKAI2a
BtKAI2_b_qR1	GCATTTAATTTCGCTAAAACTCTTG	BtKAI2b
BtKAI2_c_qR1	GAAACGATATACTCAGTACTTACCAC	BtKAI2c
CACS_qF	ACTCAGGAAGGTGTACGGTCA	Designed against At5g46630
CACS_qR	TGCATTTGGAACAGGTTTGT	Designed against At5g46630
BtCACS_qF	ACTCAGGAAGGTGTACGGTCA	Designed against At5g46630
BtCACS_qR	TGCATTTGGAACAGGTTTGT	Designed against At5g46630